Politecnico di Torino

Master's Degree Course in Biomedical Engineering

Academic year 2024/2025

March 2025

Design and fabrication of a DLP-printed flexible wearable strain sensor based on solvent-free photopolymerizable resin

Supervisor:
Prof. Stefano Stassi

Candidate:
Sara Santoro

List of Figures

Sommario

Abstract

The rapid progress in robotics and materials science has driven the innovation of flexible sensors, leading to important developments in wearable technology. These smart sensors, capable of detecting mechanical stimuli such as pressure, deformation, humidity, temperature, and light, find many powerful applications in health, medicine, sports, soft robotics, prosthetics, and human-machine interaction. Here, this thesis explores the design, fabrication, and characterization of a flexible strain sensor based on DLP solvent-free acrylate resin with ion conductivity given by lithium chloride. Utilizing a 3D printing DLP process, various sensor configurations were produced and tested to evaluate their mechanical and electrical response. The sensible layer, electrodes, and shells were studied to determine the optimal setup. The device demonstrated good mechanical properties, as well as good electrical properties (gauge factor about 1.8) and stability when subjected to cyclic tensile tests and durability tests. The applicability of this device was evaluated by detecting different signals of the human body. The results demonstrated that the performance of these sensors could be a promising starting point for the development of stable, conductive, low-cost, and easily manufactured devices. The findings suggest that these innovative sensors can bridge the gap between rigid electronics and soft human tissues.

Introduction

In recent years, the rapid advancement of technology has resulted in a growing integration of wearable sensors in daily life and scientific research. Devices that are meant to be worn directly on the human body, have a wide range of applications, including health and wellness, sports performance monitoring, medical rehabilitation, and safety at work. Their ability to gather data in real time enables them to monitor a wide range of physiological and environmental characteristics, giving useful information for diagnosis, prevention, and optimization of human activities. The wearable physiological world is characterized by softness, multi-sensory capacity, self-healing ability, and adaptability. Robots and machines are stiff, capable of perceiving unidirectional inputs, and unable to repair themselves. Taking inspiration from the human skin, which combines the desired characteristics, tactile sensors were defined as intelligent because they have functions that allow them to respond directly to mechanical, thermal, chemical, and electrical stimuli from their surroundings. The basic distinction among these sensors and typical sensors is that they are made of flexible materials, enabling them to better adapt to the irregular surfaces of soft tissue and robotics. This property makes touch sensors useful in a variety of disciplines, including wearables, soft robotics, prosthetics, and e-skin. In particular, the development of strain piezoresistive sensors capable of detecting mechanical changes has resulted in great sensitivity and the possibility of being integrated into flexible and smart devices. The piezoresistive concept is used to develop devices that can detect movement, posture changes, muscle activity, and other biomechanical changes with great precision. Given that their excellent mechanical and electrical properties, materials such as graphene and

conductive, synthetic, and natural polymers are frequently used to manufacture these sensors.

This thesis proposes investigating recent innovations in the field of wearable sensors and strain piezoresistive sensors, analyzing their applications, benefits, and challenges related to their use, device miniaturization, durability, and stability. This research focuses on the development of a printable piezoresistive sensor using a unique resin made up of a monofunctional PEGMEMA acrylate macromer, acrylic acid, BAPO INIMER as a photo initiator and crosslinker, and lithium chloride as a conducting component. This resin, free of solvents and aqueous components, has considerable benefits in terms of stability, processability, and electrical performance.

The monofunctional PEGMEMA acrylate macromer plays a key role in the resin formulation because it provides flexibility and biocompatibility, both of which are required for wearable device applications. Acrylic acid's functional groups help to produce a dense and stable polymer network through crosslinking reactions. The photoinitiator and crosslinking agent BAPO INIMER was chosen for its efficacy in UV polymerization, allowing for quick and regulated crosslinking of the resin, enhancing its mechanical qualities and long-term durability. The sensor's conductive component is given by the addition of lithium chloride (LiCl), a salt that allows efficient ionic conduction within the polymer matrix. The use of lithium chloride was driven by its unique solubility qualities and ability to improve the electrical conductivity of the polymer composite, making it suitable for piezoresistive applications. The absence of solvents and watery additives in the resin formulation provides additional benefits, including better final material purity and lower sensitivity to relative humidity, both of which can have a negative impact on sensor performance. Furthermore, the resin's modulable enables the manufacture of sensors with complicated and customizable shapes, allowing for

optimal integration into a variety of wearable devices. In the Materials and Methods chapter, it demonstrates the device's usefulness and versatility in the development of new wearable devices through a series of physicochemical characterizations and functional testing. The findings indicate that these sensors may be suitable candidates for the creation of stable, low-cost, flexible, and simply made devices. Finally, the advantages and limitations, as well as potential future advancements, are discussed at the end of this study.

1. Wearable Sensors

Wearable sensing technology has quickly grown from a scientific concept to a wide range of consumer and healthcare products. The rapid evolution of wearable sensors could be attributed to the benefits of electronic health records including low costs, ergonomic design, widespread use of smartphones, increased health awareness, and the challenge of obtaining accurate patient data. While preliminary results have been promising, further knowledge is needed to monitor physiological information accurately. Wearable sensors were first developed in the Apollo Space Program in the 1960s to monitor astronauts' health and transmit real-time data. These sensors include electrocardiograms, heated thermistors for breathing, pulse oximetry, and biosensor probes for glucose measurement. Wearable monitors gained popularity in the 1980s and were used by common people in the late 1980s. [1] Wearable electronics have grown rapidly in recent years, thanks to their flexibility and portability, which allows gadgets like electronic sensors and implantable medical devices to adhere directly to the human skin. These developments allow for the monitoring of movements and physiological data, making them valuable in medical applications such as patient health monitoring, athletics, soft robotics, biomechanics assessment, and medication delivery systems. A great deal of work has been put into the development of smart textiles, which embed electrical circuits into traditional fabrics, increasing their capabilities and allowing them to respond to mechanical, thermal, chemical, and electrical stimuli. [2] When designing wearable electronics, it is critical to consider a variety of factors, including mechanical flexibility, device scaling, basic interface mechanics and chemistries, and the preservation of high-performance materials and functional devices. Mechanical flexibility is necessary for devices that come into direct touch with specific skin regions (Young's modulus ≈130-657 kPa), minimizing discomfort and adjusting to

varied degrees of deformation caused by body movements. [3] Tactile sensors, in particular, play an important role in turning our interactions with the world, thus elastic electronic devices that replicate skin features could have major implications for prostheses and medicine. Giving prosthetic hands the ability to perceive is critical, and efforts have been made in recent decades to develop artificial skins with human-like sensory capacities. A sensor is defined as “a device used to detect, locate, or quantify energy or matter, giving a signal for the detection of a physical or chemical property to which the device responds”. [4] In the biomedical area, physical sensors detect changes in physiological stimuli and convert them into signals that may be measured or recorded. The human body provides a variety of physical stimuli during normal activity; wearable sensor systems provide opportunities for illness diagnosis, treatment, and health monitoring by quantifying and measuring the physical signals produced by the body, such as body temperature, heart rate, respiratory rate, blood pressure, skin strain, pulse oxygenation, and blood glucose. [5] So, the recent developments in sensing materials, fabrication processes, and electrical sensing techniques shown in Fig. (1.1) [6] led to physical sensing devices with special qualities like transparency, high sensitivity, extreme thinness, ultralight weight, high flexibility, and stretchability, which are the desired characteristics. [6]

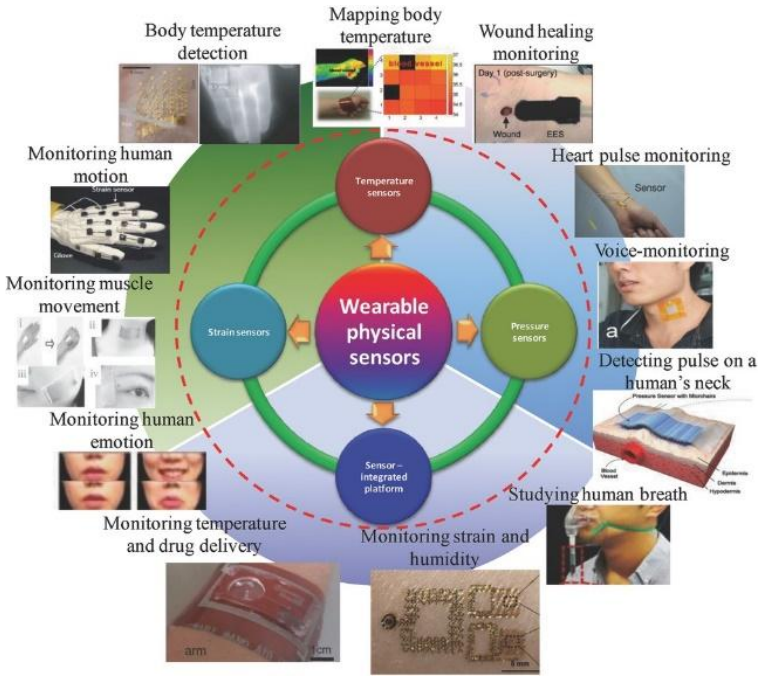

Fig. 1.1 Overview of characteristic properties of recently developed wearable physical sensors for monitoring human activity and personal healthcare using temperature, pressure, and strain sensors [6]

1.1 Flexible Wearable Sensors: features and classification

Continued innovation in medical equipment has long been a goal, but patients, particularly those in underdeveloped nations, find it difficult due to the high cost and time-consuming nature of hospital care. Researchers are developing wearable medical devices to provide economical health care while also meeting the individual demands of each patient. Global shipments climbed by 32% in 2020 to 444.7 million as a result of the integration of materials science, sensing techniques, wireless technologies, and the Internet of Things. Wearable health monitoring systems, which may monitor bodily data in real-time, are typically made up of tiny rigid circuit boards and block power supply implanted throughout the body, particularly in the hands. Despite this, these sensors lack the necessary flexibility and adaptability. [7] In this gap, flexible and wearable electronic devices are gaining popularity in artificial intelligence, healthcare, and electronic skin because of their lightweight design, ease of integration, and mechanical deformation resistance. Flexible sensors play an important role in transforming environmental stimuli into detectable signals. As a result, the development of high-sensitivity, mechanically stable, and wide-working range sensors is urgently required**.** High-performance wearable flexible sensors have been developed using various materials such as polymer materials, two-dimensional materials, carbon materials, metal materials, including hydrogels due to their biocompatibility, extensibility, and flexibility. [8] For all the above-mentioned characteristics**,** flexible sensors are essential for applications in human motion detection and personalized health monitoring. [9]

Wearable flexible sensors are electronic devices that can be worn directly on the human body to measure various physiological and environmental parameters. These sensors can be classified according to various criteria: principle of operation, type of signal measured (pressure, force, strain), materials used,

manufacturing technology, technical characteristics, and possible applications. These flexible sensors can detect physical quantities by converting mechanical stimuli into capacitance, resistance, voltage, and optics signals. Common types include pressure and strain sensors.

Pressure sensors may detect health monitoring, as they can non-invasively provide high-fidelity. This capability is crucial for mobile health monitoring and remote diagnosis in cardiovascular medicine. Flexible pressure sensors can detect force magnitude using various mechanisms, including piezoresistive, capacitive, piezoelectric, and ionotronic effects. Standard pressure sensors are often composed of rigid materials and attaching them to wearable electronics presents numerous challenges. As a result, to use pressure sensors in wearable electronics such as human-machine interfaces, biological sensors, and motion detection, a flexible sensor capable of sensitive and consistent performance, even on a curved surface, is required. Thus, the flexibility of both the electrode and the sensing layer should be ensured, as well as various electrical characteristics such as sensitivity, detection limit, reaction time, and mechanical durability. [10] Numerous studies are underway to develop flexible pressure sensors. There are two major parts to realizing flexible pressure sensors: the first is to use naturally flexible materials, and the second is to create flexibility by building specially designed structures. Flexible pressure sensors made from functional polymers such as silicone rubber have gained a lot of interest. Silicone rubber, especially polydimethylsiloxane (PDMS), is extremely flexible and ideal for wearable electronics due to its biocompatibility. Composite materials have recently been created by combining $BaTiO_3$, carbon nanotubes (CNTs), reduced graphene oxide (rGO), carbon black (CB), Ag nanowires (Ag NWs), and Ag nanoparticles (Ag NPs) to increase the electrical performance of silicone rubber. These composite materials have better electrical characteristics than bulk

materials, which can greatly increase the electrical performance of sensors. [11] Another category is wearable strain sensors to accurately detect and monitor the movements of targeted organs in the human body, such as vocal cords and joints. Strain sensors differ from silicon-based strain sensors by requiring flexibility and elasticity. Wearable strain sensors require mechanical reliability, stretchability, sensitivity, hysteresis, and linear output signal generation. [12] In Table (1.2) an overview of flexible sensors can possibly be seen. [13]

Table 1. Summary of flexible sensors for vital sign monitoring.

Biological Signals	Sensors	Flexible Materials	Features
Temperature	temperature sensor array	PANI, Ecoflex	precise response time, high resistance sensitivity
	temperature sensor array	PI, PDMS	excellent mechanical flexibility, visible transparency, self-power
	temperature sensors	PEI	ultrathin, flexible, lightweight
Blood pressure	graphene electronic tattoos	graphene	self-adhesive, low-impedance, lightweight
	piezo-composite ultrasonic sensor	PDMS	noninvasive, nonocclusive, calibration-free
ECG	ECG electrode	natural leather	convenient, comfortable, flexible, wearable
Pulse	strain sensor	PANI	flexible, low cost, wearable, simple manufacturing process
Human motion	pressure sensor arrays	PDMS, PET	flexible, wearable, multichannel
	strain sensor	conductive textile	washable, lightweight, flexible, reusable wearable
	triboelectric nanogenerator fabric sensor arrays	PDMS	flexible, stretchable, self-power
	eye-movement sensor	PDMS	highly-sensitive, skin-attachable, non-invasive
Respiratory rate	fiber Bragg gratings sensors	PI, silicone	wearable, flexible
	fiber Bragg gratings sensors	textiles	Wearable, multi-point sensing,
Glucose	sweat sensor	agarose hydrogel	noninvasive, simple, in-situ analysis
	iontophoresis integrated microfluidic epidermal biosensor	PDMS	soft, flexible, wearable, skin-mounted, non-invasive,
pH	pH sensor	composite silk fibroin film	high flexibility, biocompatibility, air permeability, biodegradability
	electrochemical pH Sensor	PET, PANI	skin-attachable, wearable, flexible

Table 1.2 Overview of Flexible Sensors [13]

In terms of materials and manufacturing, flexible sensors are developed using a range of polymers and nanomaterials, depending on their electrical, mechanical, and thermal characteristics. Some of the common polymers that have been used to devise flexible sensors are polydimethylsiloxane (PDMS),

polyethylene terephthalate (PET), polyimide (PI), and polyethylene naphtholate (PEN). Nowadays, conductive polymers, such as poly (3,4-ethylenedioxythiophene) polystyrene sulfonate (PEDOT: PSS) and polyaniline, are used to develop nanocomposite-based flexible sensors. Another possible method involves inserting conductive fillers such as carbon nanotubes, silver nanowires, and metal nanoparticles into a dielectric elastomeric matrix to form nanocomposites for stretchable conductors. [13]

1.2 Transduction mechanisms

Flexible wearable devices represent an innovative development in health monitoring and technological interaction thanks to the ability to respond to the shape of the human body and collect biometric data comfortably and quickly. A major feature of these devices is transduction, i.e. the conversion of physical, chemical, or biological inputs into usable electric signals. Transduction mechanisms include piezo-resistant and piezoelectric sensors, which convert mechanical deformations into electrical signals to monitor physical activities and movements; thermo-resistant sensors which detect temperature variations; and optical sensors which measure parameters such as heart rate and blood oxygenation. Furthermore, electrical sensors such as bioelectric impedance and electrodermal sensors assess the bioelectrical properties of the skin, and chemical biosensors detect glucose, pH, and other chemicals in body fluids. Magnetic and Hall-effect sensors and acoustic sensors like piezoelectric microphones are used to detect movements and vibrations.

Numerous studies have been conducted to improve electrical performances, such as the sensitivity, detection limit, cyclic stability, and so forth. Studies of the

active layer's materials, structure design, and fabrication methods have been actively conducted. In this section, the focus is on the sensing mechanism and design strategies according to the type of sensor. [10] The most common transduction for flexible sensors includes piezoresistive, capacitive [14], piezoelectric [15], and iontronic, which can be utilized to detect the magnitude of force, and each relies on the respective physical effects. Figure (1.3) [12] shows the most common transduction mechanisms for strain and pressure sensors.

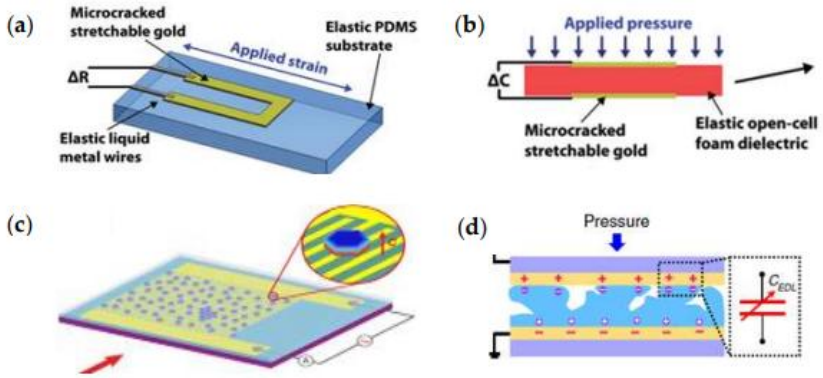

Fig. 1.3 Four typical pressure and strain sensing mechanisms. (a) Piezoresistive (b) Capacitive (c) Piezoelectric (d) Ionization [12]

Piezoresistive and capacitive sensors detect changes in resistance and capacitance caused by geometric deformation due to external forces or strain. Capacitive sensors detect pressure and strain by adjusting the frontal area and spacing of parallel plates. The detection technique is based on capacitance changes generated by the deformation or bending of pressure-sensitive mechanical parts, which modify the separation gap of the capacitor. The dielectric layer of a capacitive pressure sensor is critical to achieving high sensitivity. These sensors work based on parallel plate capacitors, with capacitance C is defined by the equation where, $C = {\epsilon 0 \epsilon r A}/{d}$, $\epsilon 0$ and ϵr are the dielectric constants of the vacuum and the dielectric layer, respectively, A is the

overlapping area of the electrodes, and *d* is the distance between the electrodes. Applying pressure causes the dielectric layer to deform, affecting d and capacitance. PDMS and Ecoflex are widely utilized dielectric materials because of their excellent deformability. These sensors' sensitivity can be improved by changing the surface of the dielectric layer with microstructures or micropillar arrays. Modifications improve deformability and affect the effective dielectric constant (ϵr), resulting in considerable capacitance variations. However, these surface alterations can collapse under low pressures, reducing the sensor's range and increasing fabrication costs. Another way to improve deformability is to construct porous structures within the dielectric layer. Particle templates, such as sugar cubes or polystyrene beads, can generate pores in polymers like Ecoflex and PDMS. Their performance can be influenced by ambient noise.

Piezoresistive flexible sensors have been extensively researched and used due to their simple construction and operating mechanism shown in Figure (1.4), comparatively simple fabrication technique, and great performance. As a result, substantial research has been conducted to develop high-performance flexible sensors. A resistive pressure sensor's sensing technique depends on resistance variation in response to applied pressure or deformations. They can present high sensitivity and wide measuring range. Resistive pressure sensors typically detect resistance between two conducting layers under applied pressure. These sensors typically use organized conductive layers. Under external pressure, the resistance between the electrodes reduces as more sections of the active layer touch one another. [12] Piezoresistive sensors, transform changes in a device's resistance into strain readings, the resistance changes can be caused by numerous factors, including the geometry of the sensing element, the contact resistance (*Rc*) between two materials, and the resistivity of a composite due to changes in interparticle separation. A material's resistance (R) is given by the equation

R=$\rho L/A$, where ρ is the resistivity, L is the length, and A is the area. The effect of geometry on piezo resistance is predominant when ρ remains constant, but L and A change with strain. Silicon (Si), carbon nanotubes (CNTs), and graphene have all shown piezo resistivity due to variations in their band structures. Organic materials can exhibit piezoresistive qualities through many methods. Typically, carrier mobility (μ) decreases with strain due to increased intermolecular separation. Piezoresistive composites often operate well near the percolation threshold of the filler material within the elastomer matrix. The filler must be evenly distributed and adhere to the matrix for constant sensing qualities. However, conductive composites typically display high hysteresis and substantial temperature-dependent electrical characteristics. Recent research by de la Vega et al. [16] demonstrates that the temperature sensitivity of CNT composites may be changed by varying the CNT concentration, potentially leading to temperature-stabilized sensors. In this case, the behavior of carbon nanotube/epoxy and carbon black/epoxy composites under dynamic load is investigated utilizing dynamic mechanical thermal analysis (DMTA) and DC electrical resistivity measurements. The results reveal a loading frequency-dependent phase shift between DC electrical resistance and mechanical elongation, with magnitude and amplitude determined by the initial electrical conductivity. Temperature sweeps show that piezo resistance varies with temperature, with network properties having a substantial impact on the piezoresistive behavior of these composites. [16] Carbon black (CB) has long been employed as a conductive filler in strain-sensing materials due to its low cost and abundance, and its piezoresistive capabilities are consistent with existing models. CNTs and graphene have also sparked interest because of their unusual electrical and mechanical properties, with anisotropic composites or films of CNTs exhibiting extraordinary sensing capabilities. In this strand of

research, to overcome limitations such as time response, noise resistance, and electrostatic modality, Chen et al. [17] created an efficient, low-cost strategy for fabricating piezoresistive pressure sensors with dense PdNP arrays deposited on flexible PET membranes, based on the hypersensitive sensitivity of the tunneling conductance of the closely spaced NP arrays to small strain. Furthermore, microstructures such as tiny pyramids have been demonstrated to improve the sensitivity of flexible sensors significantly. [13]

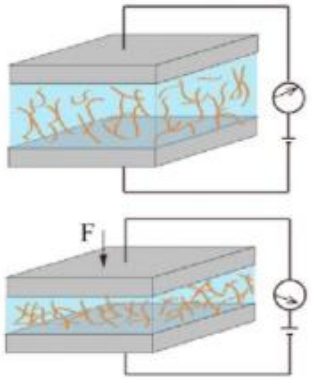

Fig. 1.4 Piezoresistive transduction mechanism [18]

In recent years, another mechanism has been behind the search for sensors, piezo ionic effect materials, such as ionic polymer composites, so show great promise for enhanced sensor technologies. Unlike traditional electronic sensors, ionotronic sensors use an electrolyte to manipulate and transport ions within the sensor under an electric field. These materials create electrical output in response to mechanical deformation by redistributing ions internally, as opposed to piezoelectric or triboelectric materials, which use dielectric or contact-induced charges. Due to their unique properties, ionotronic sensors provide remarkable electrical performance even under mechanical stress. [19] Ionotronic sensors, such as hydrogels, organ gels, and ion gels, are soft due to the high liquid phase content in their polymer matrix and can enhance

mechanical properties through intermolecular interactions, resulting in high toughness, self-healing capabilities, and strain-stiffening behavior. [20] Ionotronic sensors have remarkable mechanical properties and can be used as wearable sensors. Ionotronic sensors use a solvent to ionize inorganic salts, ionic liquid, and liquid-free in solid-state forms with mobile ions such as polyelectrolytes. [21] Each type has distinct properties based on the ion transport technique. Solvent-based ionotronic sensors exhibit strong ionic conductivity (1-10 $S \cdot m^{-1}$), that utilize polar solvents to dissociate ions and generate mobile ones within the layer. Water-based hydrogels, with over 90% water content, are a key focus in the development of iontronics. [22] The Suo group et al. have developed elastomeric hydrogels with great stretchability and toughness by combining strong covalent interactions between polyacrylamide polymers (PAAm) and weak ionic bindings between algae chains and Ca2+ ions. Strong bonds remain unbroken while stretching, increasing chain length and determining material elasticity, whereas weak bonds break. [23] One notable example is the Ionic Polymer Metal Composite (IPMC), which has received attention for its possible use in sensors and actuators. However, research on IPMCs as sensors is limited due to issues such as water evaporation, which affects sensor stability. To solve these challenges, researchers created piezo ionic sensors that use ionic liquids as electrolytes and graphene composites as electrodes to generate stable electrical signals in the absence of external power. Encapsulating these sensors enables direct connection to the skin or clothes, allowing for monitoring of a wide range of human activities. [17] Various resistant deformation sensors are based on Ionics; their constant ionic conductivity offers a continuous current flow, even under straining conditions, providing continuous monitoring of deforming variations. [19] Polymer networks significantly impact the performance of ionotronic sensors, including stretching

behavior, electrical conductivity, adhesion, Gauge Factor, and linearity. Researchers have devised strategies for modulating polymer networks to address these key concerns. Gao et al. (2023) created a double network hydrogel by combining Al^{3+} ions with chitosan (CS) and hyaluronic acid (HA) shown in Figure (1.5). This resulted in ionic coordination between the CS hydroxyl and amino groups and HA carboxyl groups, as well as hydrogen bonding among the polymers. The noncovalent, dynamic, and reversible crosslinking interactions resulted in a material with great stretchability (up to 2000%) and self-healing efficiency (97%). The remarkable mechanical quality resulted in an ISS with a GF of 4.42, 800% sensing range, and sustained performance even after 300 repetitions at 50% strain (Figure 1.5). [24] In addition, Table (1.6) presents a summary of the major characteristics of a flexible sensor based on sensing devices and elastic substrates. [17]

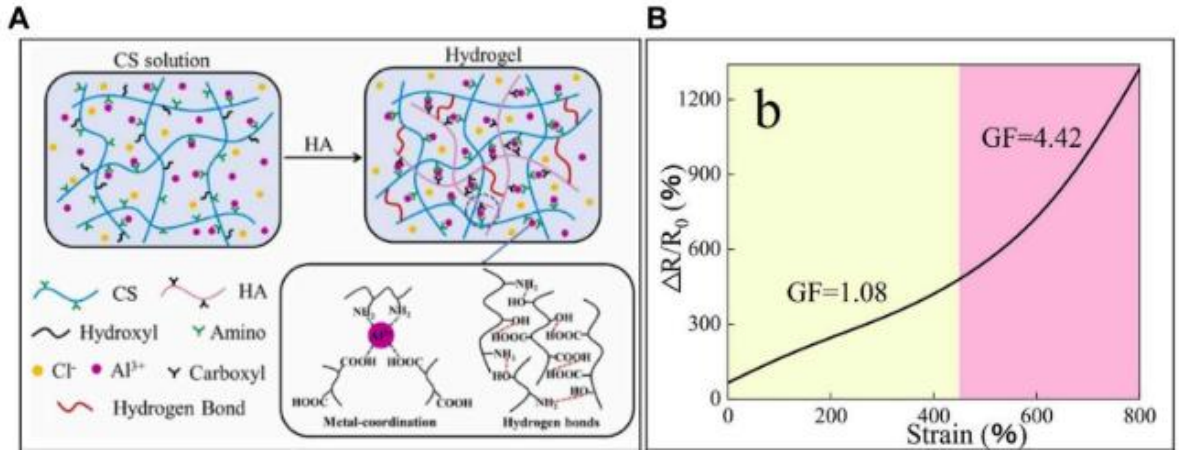

Fig. 1.5 The strategies for the enhancement of sensing performance of ionotronic sensor. (A) Schematic diagram and intermolecular interaction of Chitosan/Hyaluronic acid/Al3+ hydrogels, and (B) sensitivity [24]

Sensing Element	Substrate	Mechanism	Sensitivity	Detection Limitation
CNTs/leather	Leather	Piezoresistive	8.03 kPa^{-1}–32.42 kPa^{-1}	50 kPa
MXene/Ti_3C_2Tx	Paper	Piezoresistive	3.81 kPa^{-1}	23 Pa−30 kPa
SF@MXene	PET	Piezoresistive	25.5 kPa^{-1}	0.1 kPa–20 kPa
AM/MoS_2/Al_2O_3	Microchem SU8	Piezoresistive	0.011 kPa^{-1}	1–120 kPa
CNT and Au	Elastomer	Piezoresistive	/	1–80 kPa
Nanoparticles	PET	Piezoresistive	0.13 kPa^{-1}	0.5 Pa
Graphene oxide	Ecoflex/PDMS	Piezoresistive	0.0338 kPa^{-1}	7 mN
CB and NaCl	PDMS	Piezoresistive	5.54 kPa^{-1}	10 Pa–800 kPa
Graphene oxide	PDMS	Piezoresistive	25.1 kPa^{-1}	0–2.6 kPa
Graphene	PDMS	Piezoresistive	1.2 kPa^{-1}	5 Pa–25 kPa
Graphene/Ag	Sea sponge	Piezoresistive	0.016 kPa^{-1}	0–40 kPa
Carbon/MXene	PET	Piezoresistive	12.5 kPa^{-1}	0–10 kPa
$Ti_3C_2T_x$ MXenes	PU sponge	Piezoresistive	0.01 kPa^{-1}	9 Pa–245.7 kPa
PEDOT:PSS	Paper	Piezoresistive	1.14 kPa^{-1}	300 Kpa
CB/AP	Paper	Piezoresistive	51.23 kPa^{-1}	1 Pa
MXene/PVDF	PDMS	Capacitive	0.51 kPa^{-1}	0–400 kPa
Ferrite	Fabric	Capacitive	0.19 kPa^{-1}	0–20 kPa
Silicone/Gold	PDMS	Capacitive	0.001–0.01 kPa^{-1}	5–405 kPa
MoS_2/WSe_2	PET	Capacitive	44 kPa^{-1}	0–5 kPa
ZnO	PDMS	Piezoelectric	84.2–104.4 meV/MPa	0–1 Mpa
PVDF-HFP/PEDOT	PET	Piezoelectric	13.5 kPa^{-1}	1 Pa–30 kPa
ZnO	Cr/Au	Piezoelectric	1448–1677 meV/MPa	24.84–152.88 kPa
ZnO	Cr/Au	Piezoelectric	60.97–78.23 meV/MPa	2 kPa–3.64 MPa
$PbTiO_3$/Graphene	PDMS	Piezoelectric	9.4 × 10^{-3} kPa^{-1}	0–1.5 kPa
PVDF	PEN	Piezoelectric	25 kPa^{-1}	0.025–1.5 MPa
Conductive fiber	Paper	Iontronic	1.0 nF/kPa/cm^2	5.12 Pa–200 kPa
PVA/H_3PO_4	PI	Iontronic	220 kPa^{-1}	0.08 Pa–360 kPa
Cellulose fiber	Paper	Iontronic	10 nF/kPa/cm^2	6.25 Pa
Emim TCM	PET	Iontronic	0.43 nF/kPa/cm^2	33 Pa
Emim TCM	PET	Iontronic	29.8 nF/kPa/cm^2	100 mN

Abbreviations: Airlaid paper (AP); Active-matrix (AM); Silk fibroin@$Ti_3C_2T_x$ MXene (SF@MXene); Poly(vinylidene fluoride-co-hexafluoropropene) (PVDF-HFP), Poly(3,4-ethylene-dioxythiophene) (PEDOT), (PVDF-HFP/PEDOT); Polyvinyl alcohol (PVA); 1-ethyl-3-methylimidazolium tricyanomethanide (Emim TCM).

Table 1.6 Summary of main characteristic parameters of flexible sensors based on sensing elements and elastic substrates. [17]

1.3 Piezoresistive strain sensors, performance characteristics

Stretchable sensing elements that can maintain stable electromechanical properties under high strain are often created by combining flexible matrix materials and conductive materials. The structures and physical characteristics change when the sensing elements are subjected to external stimuli like pressure and stress. Strain sensors can be one-dimensional (1D) such as fibers, two-dimensional (2D) films, or three-dimensional (3D) hydrogels, sponges, and foams. The primary performance characteristics of flexible strain sensors are sensitivity (GF), reaction time, stability, durability, hysteresis, and other indicators. Flexible strain sensors detect four types of strain: stretching, compression, bending, and torsion. [9] For stretchable sensors to be successfully implemented in biomedical applications, the sensors should have four basic properties: (1) living flexible/stretchable, (2) exhibiting both a rapid response and recovery time (low electrical and mechanical hysteresis), (3) producing a linear relationship between strain and resistance with low electrical drift to prevent noise in the signal. The electromechanical properties of stretch sensors vary due to the variety of materials employed in their fabrication, resulting in varying test techniques and results. While the materials comprising the sensors may vary, the electrical resistance (R) and mechanical strain properties (ε) of the sensors can be correlated by calculating the gauge factor (GF), which measures the sensitivity (k) of the sensor:

Eq. 1.7

$$k = \frac{\frac{\Delta R}{R_0}}{\frac{\Delta l}{l_0}} = \frac{\frac{\Delta R}{R_0}}{\varepsilon}$$

where: ΔR = change in resistance; R_0 = initial resistance; Δl = change in length; l_0 = initial length. An increase in the ratio of the resistance to strain results in an

increase in the sensitivity of the sensor. Further, the gauge factor may be positive or negative. Because sensitivities can vary greatly depending on the materials used to make the sensors, the sensor used may be influenced not only by the signal's repeatability and sensitivity but also by its application. [25] Regarding the performance of stretchable strain sensors, different performance metrics, including stretchability, sensitivity or gauge factor (GF), linearity, hysteresis, response and recovery time, and durability, are essential for the characterization of stretchy and wearable strain sensors. Stretchability varies depending on the strain sensor used, nanomaterials, micro/nanostructures, and even the manufacturing method. Resistive sensors with high stretchability (ε = 280%) were produced using CNT thin film-PDMS composites. In parallel, percolating CNT network-silicone elastomer composites were used to exhibit ultra-high stretchy (ε = 300%) capacitive-type sensors due to the high stretchability of the dielectric layer. GFs of strain sensors are impacted by the slope of the relative change of the electrical signal, typically resistance or capacitance-versus applied strain. So, the value of GFs for stretchable strain sensors varies based on the piezoresistive mechanisms, nanomaterials, and micro/strain sensor nanostructures. [26] By modulating the tunneling resistance during stretching, CNTs-Eco flex nanocomposite-based resistive-type sensors obtained gauge factors (GFs) of 1-3. In contrast, resistive-type sensors built from AgNWs-PDMS nanocomposite demonstrated changeable GFs ranging from 2 to 14, which were regulated by the number density of the AgNW percolation network. Higher GFs were due to more effective disconnections between NW-NW links in low-density networks. Although decreasing network density increased the sensitivity of different strain sensors, it lowered their stretchability. [27] One of the primary disadvantages of almost resistive-type strain sensors is their non-linearity. For instance, the high non-linear response of strain sensors was caused by inhomogeneous microcrack

formation and propagation in thin films composed of NPs or graphene flakes. For this reason, strain sensors based on CNT polymer composites often showed limited sensitivity and non-linear electromechanical performance. The hybrid architecture of the CNTs-polymer composites enhanced both their linearity and sensitivity. Additionally, when strain sensors are subjected to a dynamic load, such as in wearable and skin-mountable applications, hysteresis becomes crucial. This hysteresis is caused primarily by interactions between nanomaterial fillers/conductive components and polymers, as well as the viscoelastic properties of polymers. AgNWs-PDMS nanocomposite sensors, for example, exhibited considerable hysteresis at high stresses but minimal hysteresis at strains of up to 40%. Strong interfacial binding between elastic nanomaterials (e.g., graphene and CNTs) and polymers can considerably improve strain sensor performance. However, elastic nanomaterials with poor binding might slip within polymer matrices during extreme stretching and fail to promptly return to their former places following strain release, resulting in high hysteresis. Rigid nanomaterials, such as metal NWs, require low interfacial adhesion with polymers to return to their original places after release.

1.4 Promising state-of-the-art wearable sensing applications

This section presents the state-of-the-art possible applications of wearable sensors. Flexible tactile sensing technology is now widely used in a variety of applications, including intelligent robots, human-machine interfaces, virtual reality, medical treatment, and health monitoring. Flexible tactile sensors are constantly improving to meet the needs of new applications, including flexibility, sensitivity, sensitivity, sensing range, reaction time, stability, and other performance factors. Optimizing the sensing material and device architecture resulted in an ultra-thin sensor without sensory interference. Bluetooth and near-field communication technology have made wireless tactile sensors possible. A sensor array was created to decode facial strains using machine learning. Likewise, a sweat sensor was designed to detect blood glucose, nicotine, and other health information. [1] A highly successful application is electronic skin (E-Skin) like a flexible wearable touch switch. The human skin is a remarkable organ, consisting of an adaptable network of sensors that provide temperature, pressure, and touch information to the brain, allowing us to safely navigate our environment. This intuitive capability stems from specialized receptors within the skin that convert physical stimuli into electrical signals, which are then processed by the central nervous system for interpretation by the somatosensory cortex. Mimicking this sophistication in artificial skin, known as sensitive skin, smart skin, or electronic skin (e-skin), holds promise for applications ranging from autonomous robots to advanced prosthetic devices with enhanced sensory perception, so electronic skin is a flexible sensor device that simulates how the human skin detects and stores external stimuli signals. [1][28] In Fig. (1.8) a summary of the evolution of e-skin. [29]

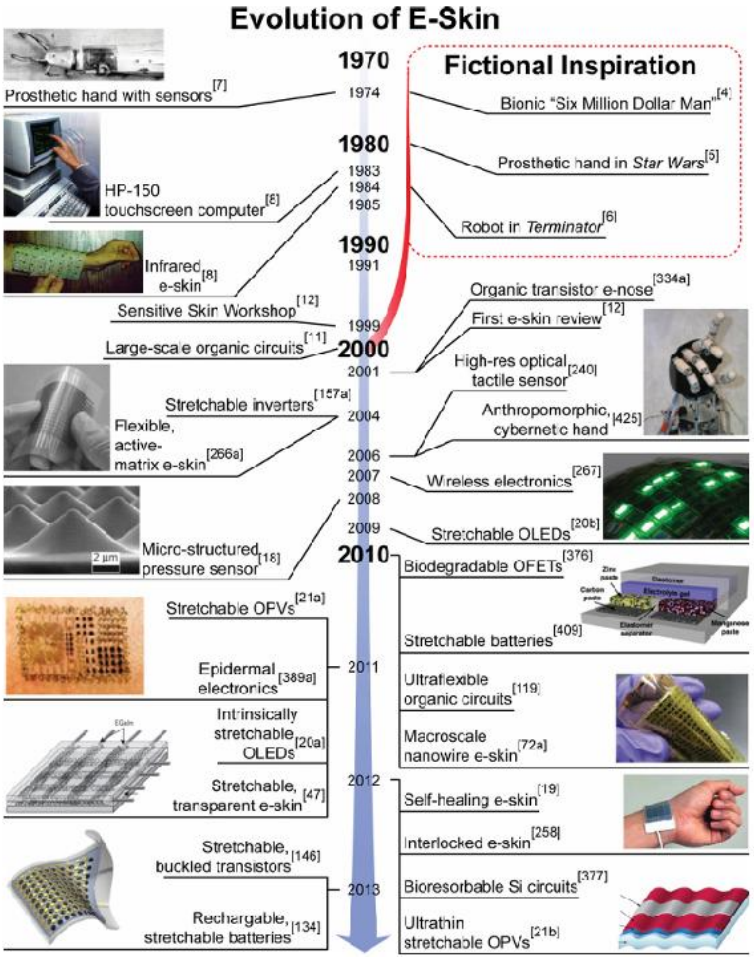

Fig. 1.8 A brief chronology of the evolution of E-skin [29]

Thanks to its simple structure, mechanical flexibility, and large-scale manufacturing capacity, it can conform to complex surfaces and adhere to devices to detect the basic properties of objects. So, to replicate biological features, the e-skin must have several tactile functions simultaneously to mimic the human skin, detecting pressure, temperature, humidity, and other environmental information. Researchers can incorporate chemical and biological sensors into flexible substrates to detect specific species in gases or liquids. Furthermore, e-skins can include temperature sensing as well as other features such as biocompatibility, self-healing, and self-powering, which increases their utility and possible uses. Recently, these sensors, made from soft and elastic materials, can monitor health by detecting pulse, body temperature, and blood

sugar. They are used in wearable devices for health monitoring and in robotics to allow patients and robots to perceive the outside environment. The e-skin combines new materials and structural designs identifying the geometry, position, structure, and hardness of the objects touched. In addition, it senses tension, strength, cutting, torsion, bending, and vibration, improving environmental detection capabilities. Considerations about the design of e-skin expect material selection, and processing methods for manufacturing elastic and flexible devices in addition to mechanical compliance, good electrical performance, and compatibility to create highly functional and cost-effective devices. [29] Despite this, most e-skins are susceptible to bacterial infections, posing serious dangers to human health. Thus, creating an e-skin with dual sensory signals and antimicrobial capabilities is incredibly useful. In Fig. (1.9) the recent progress in Electronic Skin. [30]

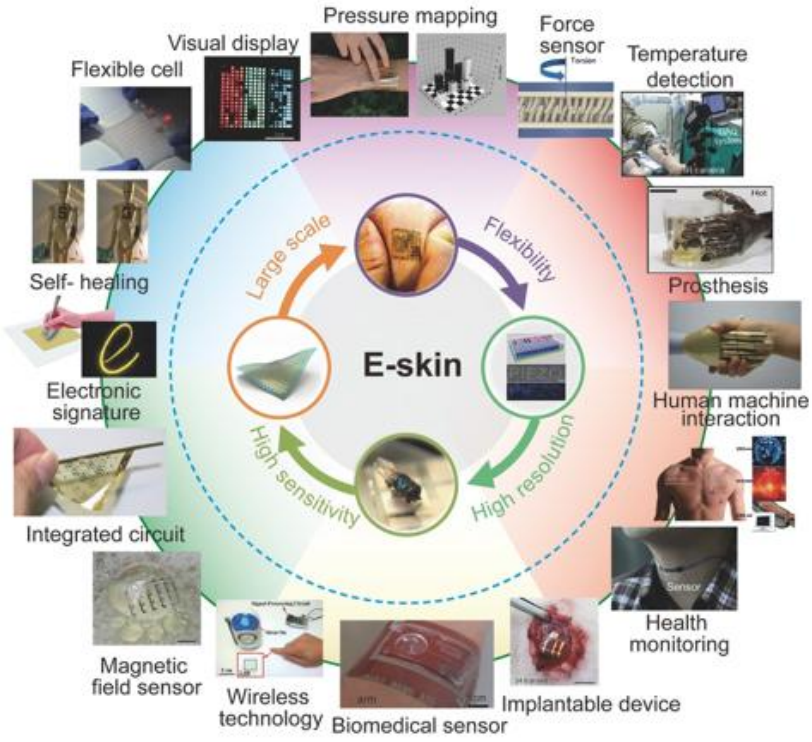

Fig. 1.9 Characteristic properties and diverse functions or applications of recently developed devices for e-skins [30]

Now it presents some works in the literature that have reported powerful results. A freezing technique was used to make a dynamic supramolecular hydrogel including conductive graphene (G), biocompatible polyvinyl alcohol (PVA), self-adhesive polydopamine (PDA), and antibacterial silver nanoparticles synthesized in situ. This hydrogel's hierarchical network structure has a tensile strength of 1.174 MPa and a 331% extension, making it excellent for flexible e-skin applications. The PVA-G-PDA-AgNPs composite hydrogel, which adheres to numerous surfaces and is highly conductive, has been successfully used as a strain sensor to detect various human motions. [29] Because of their low cost and adaptability for large-area arrays, organic and polymer-based active materials (OSs and CPs) are promising for e-skin applications. Despite performance limits, OSs provide chemical and physical qualities that may be customized by molecular structure modifications, allowing for more control over deposition conditions and shape and stability optimization for e-skins. Their solubility can be adjusted to make them compatible with large-area solution-processing techniques including spin coating, screen printing, and inkjet printing, allowing for low-cost manufacture on flexible substrates. Wearable flexible strain sensors can detect, acquire, and continuously transmit physiological signals such as heart rate and respiration, sudor sensors, pulse, and blood pressure (human physiological signal monitoring) without being influenced by daily activities, improving personalized medical treatment. The performance of these adaptable sensors when employed as dry electrodes has been demonstrated in the development of printed and flexible electrocardiographic (ECG) electrodes. These electrodes, made with silkscreen process and silver flake ink, detect ECG impulses without needing gel on the skin. Kwan et al. used metal nanoparticles to create wearable, flexible sensors for heart rate monitoring. [13] An innovative

work developed to distinguish distinct facial expressions, On et al. positioned flexible stress sensors on the forehead, brows, nose, tail, and corners of the mouth. Thanks to multichannel connectivity, these sensors can recognize eight major facial expressions: grin, surprise, sadness, fear, irritation, anger, and relaxation to track human body movements. This ability to recognize can be used in medical contexts like physical therapy and rehabilitation. Body motion sensors for the skin constructed with a triboelectric nanogenerator (TENG) can be classified into several types based on the triboelectric materials utilized. The first type is built with stretchable materials, such as rubber and silicone elastomers. Yin et al. a TENG based on elongated rubber that utilizes triboelectricity between a stretchable rubber and an aluminum film (Al), as shown in Figure (1.10) (a)–(c). [29]

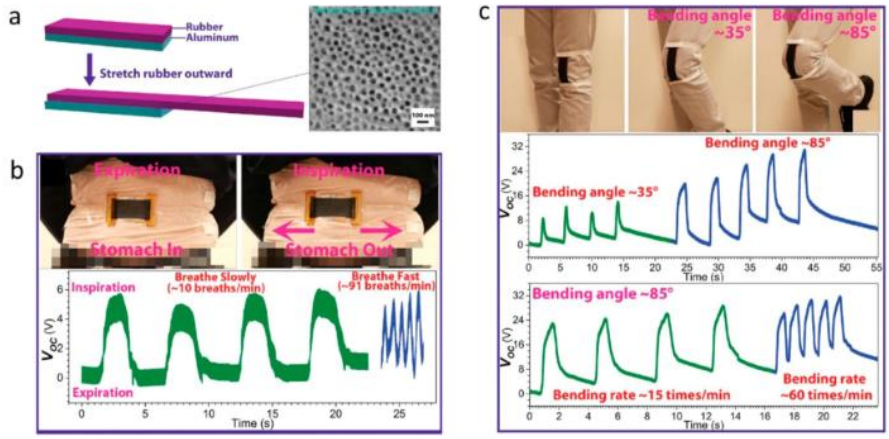

Fig. 1.10 a) Device structure of the stretchable rubber based on a triboelectric nanogenerator (TENG). (b) Images and electrical outputs of the TENG on the abdomen during expiration and inspiration. (c) Optical images of the device on the knee at different bending angles and voltage responses when bending the knee at different angles and different rates. [29]

Another area of interest is soft robotics. Soft strain sensors are useful for exoskeletal devices because they can precisely measure joint angles and body

locations. However, it has been observed that measured joint angles can diverge at higher loading rates, such as those encountered while running. Assistive devices like exoskeletons can help people with motor impairments by compensating for reduced motor function and increasing mobility. In addition, sensors can improve the safety of interactions between humans and robotic systems. Specifically, robotic systems outfitted with haptic sensors can improve user safety during close human-robot interactions, frequently in conjunction with soft actuators, to provide a feedback system that records the sensor signal. Yang et al. used a conductive elastomer sensor to detect the position of a robotic gripper; robotic grippers with embedded sensors may better align items and alter forces after contacting the object, as shown in Figure (1.11). [8][31]

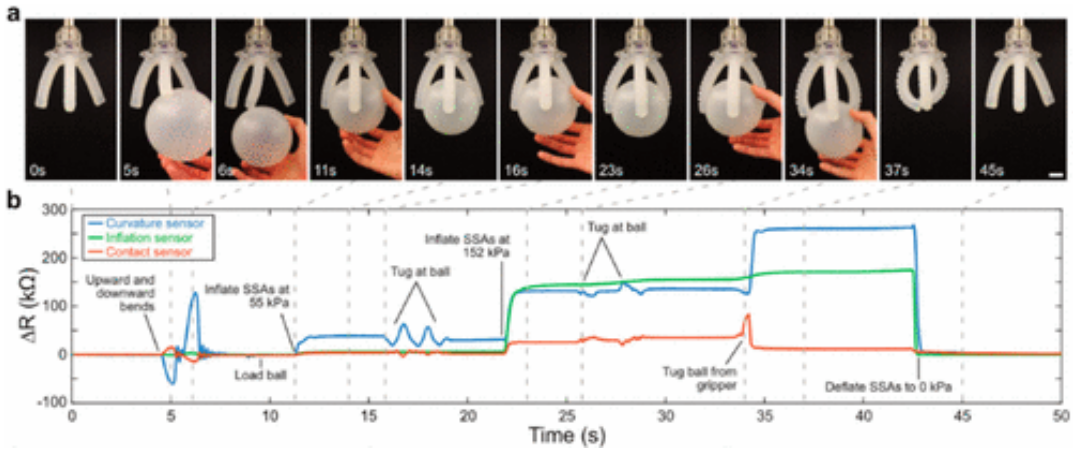

Fig. 1.11 Soft robotic grippers with Eco flex-based deformation sensors provide somatosensory feedback. (a) Images of an interaction process between a ball and a soft robotic gripper, (b) Time-dependent ΔR values for each sensor during the interaction sequence are described in (a). [31]

In addition to their uses in wearable strain sensors, wearable sensors have the potential to detect wound infections. Persistent inflammation, which is frequently caused by bacteria and other microorganisms, has a considerable impact on chronic wound healing, necessitating long-term care and extensive medical resources, imposing a significant financial burden on families and

society alike. Detecting and controlling recurrent wound infections is critical to lowering patient mortality. Flexible wearable sensors have gained popularity due to their convenience in health assessments and real-time monitoring of physiological signals. These sensors can detect biophysical and biochemical signals in biological fluid, making them ideal for wound diagnosis. Flexible wearable sensors, such as fluorescence, colorimetry, and electrochemistry sensors, have shown the ability to detect microorganisms at wound sites in real-time. Traditional bacterial detection methods, such as bacterial culture, PCR, and ELISA, necessitate laboratory conditions, specialized equipment, and skilled staff. In contrast, flexible wearable sensors provide rapid in-situ detection, are simple to use, and limit the possibility of cross-contamination. These sensors can be developed using biocompatible, degradable, breathable, flexible, stretchable, and self-powered materials, such as hydrogels, cellulose-based nanomaterials, and triboelectric nanogenerators. However, flexible wearable sensors also face challenges in providing robust, stable, accurate, and continuous monitoring. [32]

2. Piezoresistive strain light-cured sensors

2.1 Introduction to polymers photosensitive and 3D printing

In the last two decades, wearable (bio)sensors driven through emerging three-dimensional (3D) printing technologies are currently considered the next-generation tools for various healthcare applications due to their exciting characteristics such as high stretchability, super flexibility, low cost, ultra-thinness, and lightweight. Many of these printing technologies are being gradually developed due to significant improvements in printing processes, print resolution, print speed, feature size, and printable material compared to traditional layer fusion. These characteristics make them suitable for wearable devices, creating unique structures to meet the desired 3D output, as shown in the Fig. (2.1) [33]

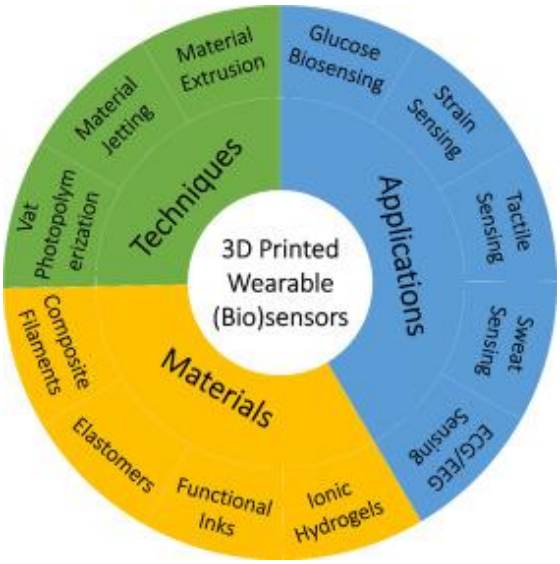

Fig. 2.1 Overview about 3D Wearable sensors [33]

3D printing is a bottom-up additive method that deposits material or ink on layers to form a solid 3D item. [34] According to recent publications, three key technologies for generating 3D-printed strain sensors include fused deposition

modeling (FDM), direct ink writing (DIW), and digital light processing (DLP). Digital Light Processing (DLP) is a key 3D printing technology because of its quick printing speed, excellent resolution, and low cost. The DLP-printing technique uses ultraviolet light to irradiate precursors in a combination of photocurable resins, crosslinkers, and catalysts. These components are chosen depending on the strain sensor setups and the crosslinking methods, such as radical polymerization and cationic photocuring. [35] The photochemical process that occurs during printing is photopolymerization which transforms a liquid resin into a solid material by irradiation with UV or visible light. The resin is composed of a mixture of monomers and/or oligomers, a photo-initiator, and additives such as dyes or solvents to optimize the process. The radiation employed supplies the initial energy to start the reaction and does not interfere with its propagation or termination. Photoinitiators are organic or inorganic substances that are thermally stable and capable of absorbing substantial amounts of light at UV or visible wavelengths. Their function is to convert the energy of incident light into chemical energy in the form of intermediate reagents like radicals or excited states. To achieve high quantum efficiency, photoinitiators must have high absorbance at the appropriate wavelengths and are frequently activated by UV radiation with wavelengths ranging from 300 to 400 nm. Photopolymerization can take place at room temperature or below, and formulations can be solvent-free, making the process efficient and adaptable. [36][37] In particular, in DLP printing (in situ crosslinking), photoinitiators generate free radicals, which encourage the polymerization of monomers and prepolymers, catalyzing polymerization and curing resins. The chemical characteristics of the mixture influence the final properties of the polymer and the kinetics of grating, with aromatic chains producing rigid materials and alkyl chains resulting in flexible materials. Multifunctional monomers form three-dimensional networks that improve the

mechanical properties of the polymer. Too many oligomers increase viscosity and impede polymerization, whereas too many monomers degrade mechanical characteristics. Multifunctional acrylic and methacrylic resins, which are used for their rapid reticulation kinetics, have a high-volume withdrawal that can impair resolution. Methacrylic resins, which have a smaller retreat but a slower polymerization rate, are frequently used with acrylic resins to balance these qualities. So, photopolymerization requires a photo-initiator that, by absorbing light, generates reactive species to initiate polymerization, divided into three phases: beginning, propagation, and termination. The photoinitiator absorbs energy, and generates free radicals that react with monomers, causing polymer chains to grow. Termination occurs when two radical chains meet, forming longer chains or two chains of similar length. Oxygen inhibition, which slows reticulation kinetics and can leave a sticky surface, is a common problem, to overcome these solvents/dyes are often added to the mixture to improve the rheological characteristics and performance in 3D printing. However, the growing demand for flexible electronic devices involves the creation of soft, conductive materials with distinct features and functions. The first phase of DLP 3D printing shown in the Fig. [38] entails producing digital models with scanners or computer software, usually in stereolithography (STL) file format. STL files provide substantial triangular coordinates to recreate the surfaces of printed items, with the end product's resolution proportionate to the number of coordinates. The last stage, "slicing," includes utilizing software to break the digital 3D models into multiple layers. The laser scans the surface of the liquid photosensitive resin inks, curing the precursors at specified spots. After producing the first layer, the printing platform elevates vertically, allowing the uncured liquid resin to cover the cured materials. This procedure continues layer by layer until the 3D structure is

completely produced. [35][39] Steps for photopolymerization are shown in Fig. (2.2) [33]

$$PI \xrightarrow{hv} PI* \rightarrow R\bullet \qquad Inizio$$
$$R\bullet + M \rightarrow R - M\bullet$$
$$R - M_k\bullet + M \rightarrow R - M_{k+1}\bullet \qquad Propagazione$$
$$M_{k-n}\bullet + M_n\bullet \rightarrow M_k \qquad Terminazione$$
$$M_{k-n}\bullet + M_n\bullet \rightarrow M_{k-n} + M_n$$

Fig. 2.2 Steps about photopolymerization [33]

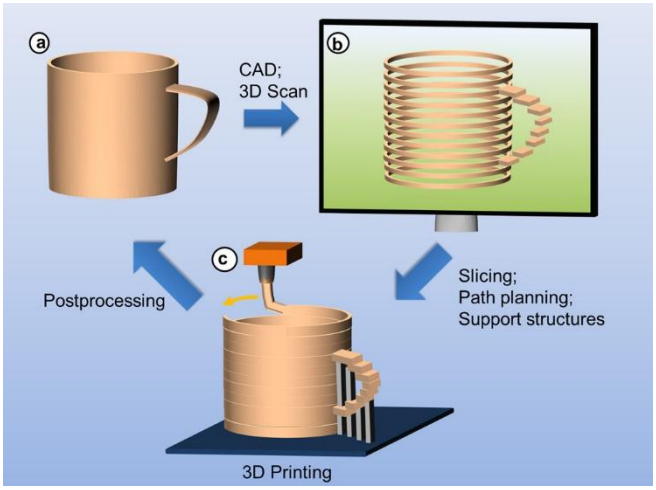

Fig. 2.3 Basic principles of additive manufacturing. (a) Development of product idea that is transformed into digital data using CAD (b) preprocessing of model data (c) and additive manufacturing of model or product [38]

Methods	Illustration	Principle	Pros	Cons
DLP		In situ photocuring	✓ High resolution ✓ Intricate fabrication	✓ Weak strength ✓ High cost
FDM		Fusion-driven restacking	✓ Fast printing ✓ High strength	✓ Rough surface ✓ Weak interaction
DIW		Ink extrusion	✓ Material diversity ✓ Low cost	✓ Post-processing ✓ Nozzle clogging

Tables 2.4 Principles, features, and typical research on 3D-printed strain sensors, offering a complete overview of advancements and approaches [38]

2.2 Conducting polymers, hydrogels, and ion gels

The conductivity of ionic-conducting hydrogels is caused by the directional movement of free-charged ions embedded in the hydrogel network. Ionic-conductive hydrogels have flexibility like biological tissues, making them ideal candidates as soft substrates for flexible wearable electronic devices. [5] Electronic conductive hydrogels (Fig. 2.5) are novel materials that combine a conductive filler matrix with a hydrogel matrix studied as elongation sensors due to their high conductivity, elasticity, and speed of recovery. Recently, a new class of conductive materials has emerged, including hydrogels, ion gels, and polyionic elastomers. These materials use charged ions to transmit electrical signals, offering high extensibility, transparency, and biocompatibility.

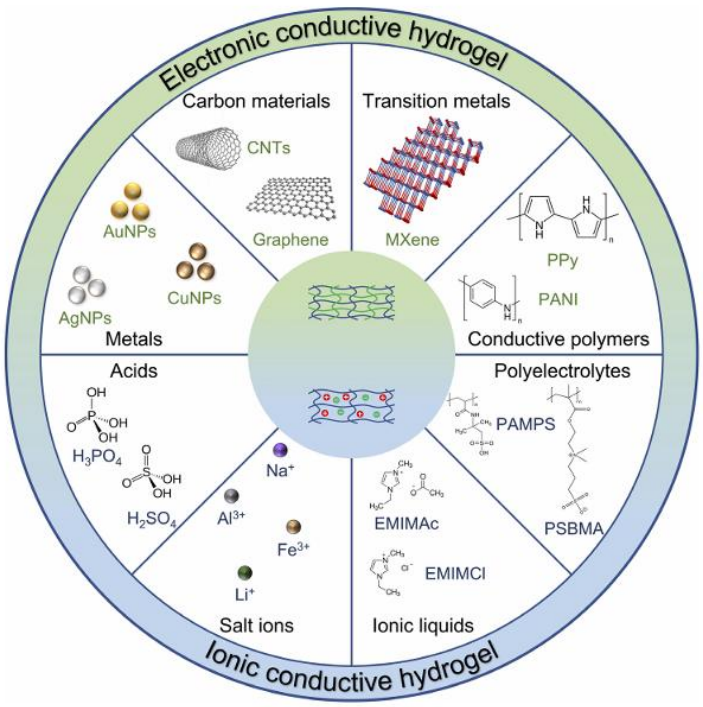

Fig. 2.5 Representative strategies for synthesis of conductive hydrogels. [5]

Metal fillers like nanoparticles (NPs) and gold, silver, and copper nanowires can be included in conductive fillers to increase the hydrogel's electrical conductivity and mechanical qualities. At the same time, carbon-based materials like carbon nanotubes and graphene are valued for their excellent conductivity, environmental stability, and biocompatibility, making them ideal for flexible sensors and wearable electronics. Conductive polymers, such as polyanyline (PANI), polypirrole (PPy), and PEDOT, have variable conductivity and are frequently integrated into hydrogels for biomedical applications due to their biocompatibility. However, the key challenge is compatibility between metals and polymers, as variations in chemical characteristics can cause metal agglomeration and phase separation in polymer networks. Despite these challenges, innovative approaches like the insertion of hybrid nanoparticles and the use of complex patterning have been proven to increase both hydrogel conductivity and mechanical properties. These advancements make conductive hydrogels a possible solution for a wide range of applications, from flexible sensors to medicinal devices, however further study is needed to maximize their stability and compatibility. It’s possible to observe an overview of the case study cited previously shown in Fig. (2.6). [5]

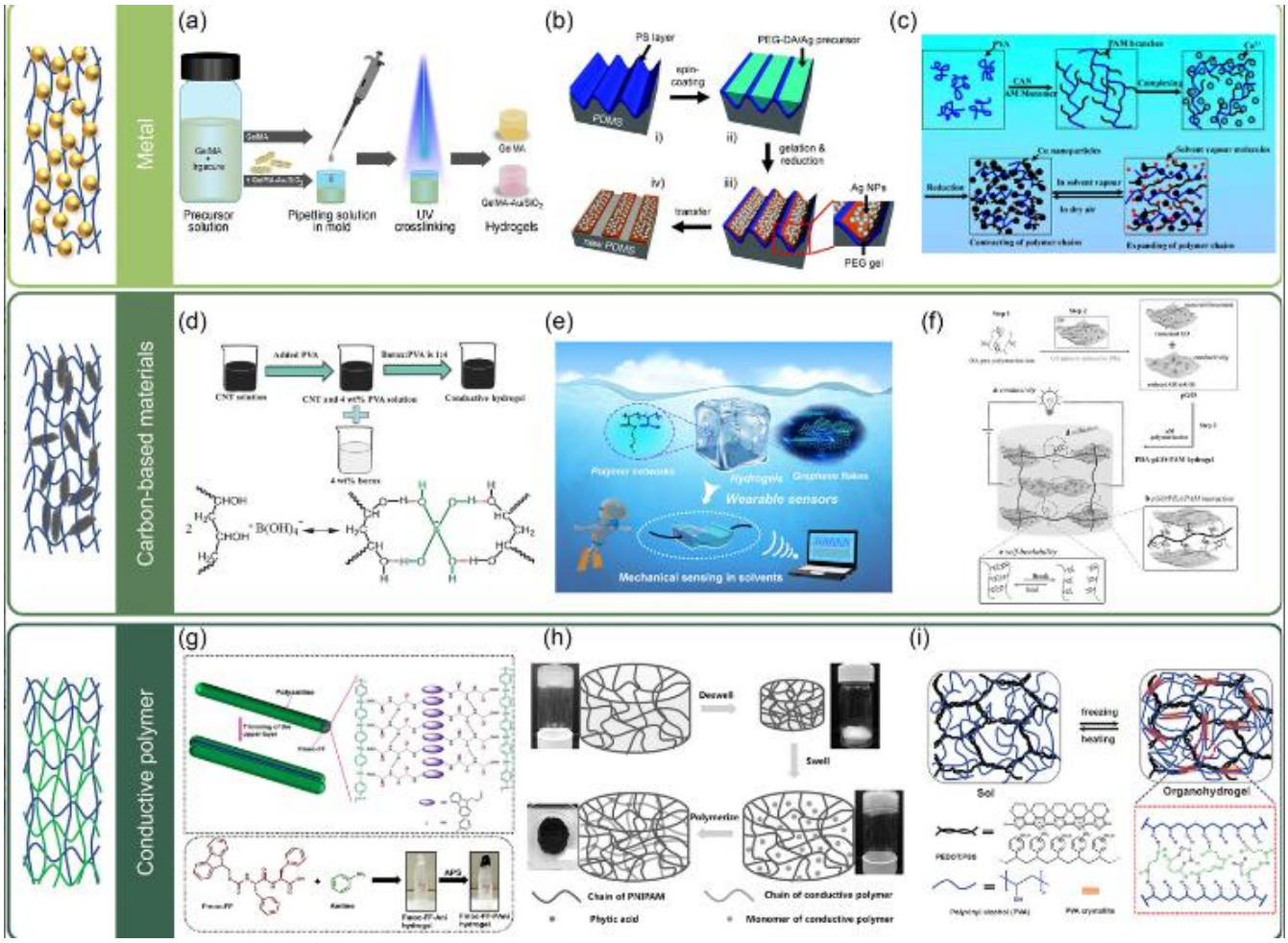

Fig. 2.6 Representative electrically conductive hydrogels based on different conductive fillers, graphene-based conductive hydrogels, and conductive polymers [5]

Flexible hydrogels, often prepared with poly (N-isopropyl acrylamide) (PNIPAm), poly (hydroxyethyl methacrylate) (PHEMA), and PAAm, are one class of hydrogels. These materials are distinguished by their quick swelling rate and strong water absorption capacity. Another category includes polyethylene glycol (PEG) hydrogels, which are known for their strength and high-resolution printability. [40] The co-crosslinking of flexible PAAm with strong polyethylene glycol diacrylate (PEGDA) hydrogels can result in complex structures that can endure large deformations and have tunable elasticity, outperforming standard 3D-printed photopolymerizing hydrogels. Furthermore, adding ionic salts such as sodium chloride, to the PAAm-PEGDA hydrogel matrix improves water retention and ionic

conductivity, making it suitable for wearable devices. This combination results in microstructures with extraordinary features including elasticity, extensibility, and transparency, which are suited for the creation of highly sensitive sensors. [41] PAAm, PHEMA, and PNIPAm hydrogels have received a lot of attention in literature since they are PEG-based and have great printability and resolution. The most popular conductive printing ink in ionic skin is PAAm + hydratable salts (LiCl, NaCl, and MgCl2). Some ionic inks present Young's moduli of 0.01 MPa, which is significantly lower than human skin's elastic modulus of 0.15-0.25 MPa. To advance the development of ionic skin, an ionic conductive with elasticity like human skin and high-resolution SLA or DLP 3D printing is required. [40] Additionally, incorporating the highly hydratable salt magnesium chloride ($MgCl_2$) into the PAAm-PEGDA network shown in Fig. 2.7 enhances the hydrogels' ionic conductivity and water retention abilities. These features make the co-hydrogel an ideal candidate for use as a transparent, stretchable, and elastic electrode, designed with an optimized microstructure to improve the sensitivity of ionic skins.

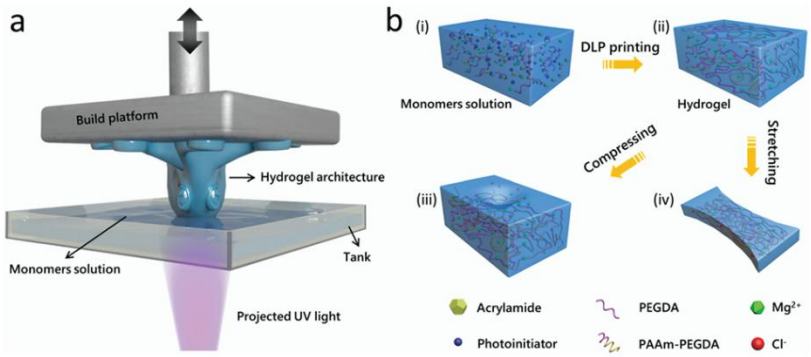

Fig. 2.7 Schematic diagram of the manufacture of the conductive PAAm–PEGDA hydrogel. (a) Fast bottom-up fabrication of a high-resolution PAAm–PEGDA architecture using a commercial DLP printer. (b) Schematic polymerization mechanism of a PAAm–PEGDA hydrogel network. [42]

The printed conductive hydrogel is flexible, elastic, almost transparent, precise, and electromechanically stable, making it suitable for use as a microstructure's current collector in wearable devices. The capacitive sensor, sandwiched between two layers of structured hydrogel film, detects static and dynamic pressures and strain with excellent sensitivity and a low limit of detection. Its enhanced features include acquiring high-fidelity body signals from many skin locations, such as finger bending tracking, and pulse waveform monitoring. The use of 3D-printed ionically conductive hydrogels as structured current collectors offers a versatile and promising solution for enhancing sensitivity. As shown in Fig. (2.8), the capacitive sensor was attached to a straight finger and, during finger bending, it was simultaneously stretched and compressed. The capacitance was measured as the finger cyclically, showing four representative cycles. Additionally, a photograph shows the sensor applied to the throat to detect larynx vibrations while pronouncing the words "Hi" and "Sensor." The capacitive sensor was also used to monitor the radial artery pulse of the human body. The measurement of the radial artery pulse wave showed results under both normal conditions (68 beats per minute) and after exercise (92 beats per minute). [43][44]

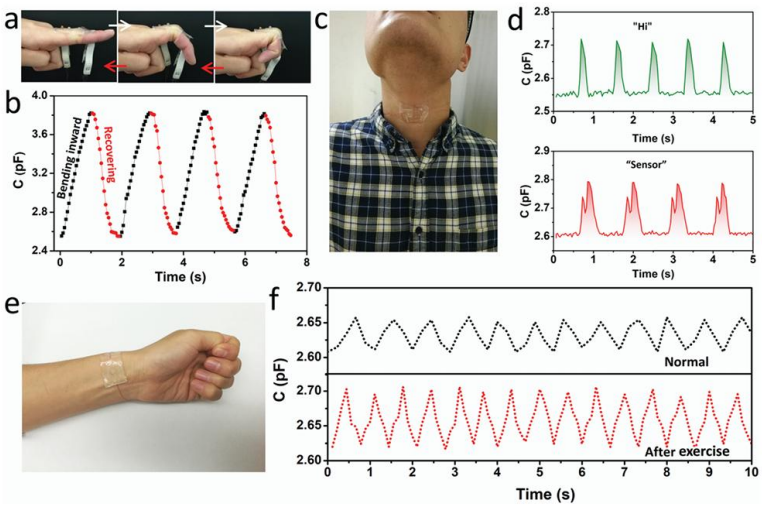

Fig. 2.8 Wearable devices to detect human motions and physical signals [41]

This work led to an important approach combining skin-like hydrogels with 3D printing technology simplifies and enhances the designability of fabricating high-sensitivity sensors. So, the method for synthesizing 3D printable co-hydrogels is versatile, allowing the printing of various ionic conductors by selecting two photo-curable hydrogels with different mechanical properties (such as PEGDA and NIPAM, or PEGDA and PHEMA), adjusting the monomer ratios, and optimizing the printing parameters. As previously discussed, 3D printing has recently sparked significant research interest in producing electrically conductive objects made from polymer nanocomposites. The ink employed was a combination of photopolymerizable resin and multi-carbon nanotubes (MWCNT). MWCNT concentrations and print parameters were investigated to determine the optimal conductivity and print quality. It is discovered that a 0.3% by-weight MWCNT charge in the resin matrix can achieve a maximum electrical conductivity of 0.027 S/m while remaining within the resin viscosity limit, allowing for outstanding print quality. Nanocomposites printed with MWCNT have electrical conductivity, making them suitable for usage as intelligent materials and structures with deformation sensitivity and shape memory. [45]

2.3 Limits of sensors based on hydrogel

This section discusses some of the limitations presented by hydrogels. Their mechanical properties and fatigue resistance are not ideal for long-term sensing applications due to the limitations that will be described below. For example, their softness and conductivity can be compromised by extreme temperatures. In some cases, a physically cross-linked double network has been proposed to improve their mechanical properties, although hydrogels still suffer from cyclic softening and strain dependency. A notable example in the literature of iono gels describes the preparation of polyacrylic acid/poly(3,4-ethylenedioxythiophene) (styrene sulphonate) (PAA/PEDOT) iono gels by a simple one-step method. These ion gels, formed with PAA as monomer, PEDOT as conductive polymeric filler, and water and IL (ionic liquid) as solvents, exhibit excellent mechanical properties, strong adhesion to various substrates, and impressive freezing resistance due to the inclusion of [BMIm][BF4]. [46]

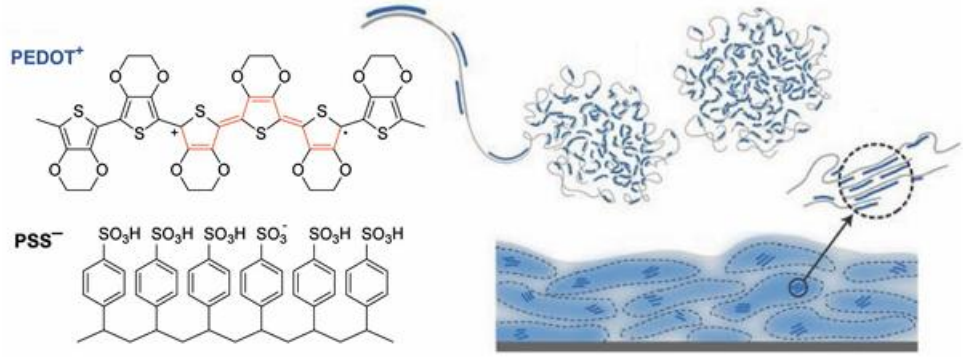

Fig. 2.9 Chemical structure of PEDOT: PSS, its formation of colloidal gel particles when dispersed in water, and microstructure of the resulting films with PSS-rich domains (gray) and PEDOT: PSS-rich domains (blue). [46]

These ionogels demonstrate high sensitivity and fast response as strain sensors but can effectively detect temperature changes. Nevertheless, hydrogel-based conductors for wearable sensors encounter limitations due to their high-water content, which freezes below zero degrees Celsius and evaporates in dry conditions (dehydration). To mitigate this problem, large quantities of salts, such as LiCl, have been incorporated into hydrogels to prevent freezing and evaporation. However, an excess of salt ions can compromise the photopolymerization efficiency of pre-hydrogels and degrade the mechanical properties of molded hydrogels. The antifreeze and anti-drying properties of molded gels were studied by examining weight loss and changes in mechanical properties in different environments. Ethylene glycol, a low-volatile diol solvent, served as an antifreeze and solvent for DLP printing ink, improving antifreeze and anti-drying properties. Designing gels with exceptional antifreeze and anti-drying properties remains a major challenge. [9][47]

To overcome some limits, a valid possibility is about ionic conductive elastomers (ICEs) emerging as promising materials for flexible electronics due to their solvent-free nature, which offers good stretchability, conductivity, and thermal stability. These properties make ICEs suitable for various ionic devices like touch sensors, ionic skin, and triboelectric nanogenerators. However, current manufacturing methods for ICEs are limited to molding and casting, resulting in simple bulk geometries. Three-dimensional (3D) printing, especially digital light processing (DLP)-based printing, offers the potential to produce more complex ionic devices. Recent advancements include the development of UV-curable ICEs compatible with DLP-based 3D printing, enabling the creation of flexible tactile sensors with high sensitivity. In comparison to ionic conductors based on hydrogel, UV-ICE has greater physical stability over a wide temperature range. Figure (2.10j) depicts the results of differential scanning calorimetry (DSC), which

show that the thermal transition temperature (Tg) of the UV-ICE campione is -49.4 °C. Above this temperature, the UV-ICE camp behaves similarly to the gomma. As shown in the insert of Figure 10 j, the polyacrylamide (PAAm) hydrogel crystallized at -30 °C after 15 minutes, but the UV-ICE sample remained unchanged. The thermogravimetric (TGA) analyses shown in Figure (2.10k) show that the UV-ICE sample is stable at temperatures below 200 °C, with no significant weight loss. [48]

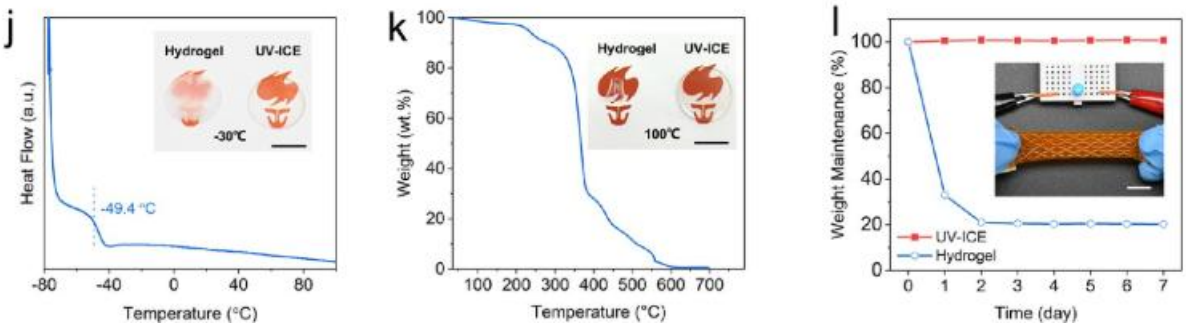

Fig. 2.10 UV-ICE versus PAAm hydrogel. [48]

When comparing the stability of the drug PAAm and the UV-ICE at 100 °C, the inserts in Figure (2.10k), the UV-ICE sample remained constant, however, the drug PAAm had a significant decrease due to water loss. Furthermore, unlike hydrogel, the UV-ICE printed structure demonstrated minimal mass loss due to the lack of solvents and maintained excellent resistance and electrical conductivity after being left at room temperature for a week. Another possible method for fabricating is using a solid-state conductive iono-elastomer (SCIE) that can be rapidly cured with light, facilitating high-resolution 3D printing of soft ionic conductors with customizable designs like microcircuits and intricate lattices. Printed SCIE-based building blocks demonstrate exceptional properties, including high Young's modulus, excellent stretchability, sustained conductivity across a broad temperature range, elasticity, and fatigue resistance even after

extensive use. These characteristics set SCIE apart from traditional printable ion-conducting materials, enduring 80,000 compressions over 10,000 cycles. Moreover, we demonstrate the capability to create 3D flexible tactile sensors with enhanced sensing capabilities by shaping SCIE-based constructs. For instance, gyroid-based piezoresistive sensors and gap-based tactile sensors exhibit sensitivity 44 and 3.7 times higher, respectively, than their bulkier counterparts. Notably, our tactile sensors offer significantly superior sensitivity compared to hydrogel/elastomer-based ion-conducting sensors. Additionally, the combination of inherent traits such as high conductivity and hydrophilicity with adaptable topological structures enabled by 3D printing positions SCIE for diverse applications including mechanical metamaterials, cellular fluidics, and soft robotics. [49]

2.4 Acrylate and methacrylate to 3D printing: an overview

The most common acrylic polymers used in sensor applications include polymers made from acryl or methacrylic acid esters, acrylamide derivatives, and copolymers. Acrylic polymers are widely employed as sensory materials because of their versatility and the ability to accommodate a wide range of sensor units chemically bonded to their structure. [50] A mechanically adjustable acrylic polymer would be made up of a few unique base monomers or oligomers, maybe with the addition of a crosslinking agent. Such solutions have been effectively used in tissue engineering as substrate coatings capable of simulating a wide variety of mechanical tissues. Fluid dynamic requirements during the 3D printing process, particularly the viscosity of the polymer, have delayed the development of a comparable system for readily adjusting the elastic module of a printable acrylic resin. Current resins may provide a wide variety of elastic modules; however, soft, and hard polymer combinations are often composed of different unique acrylate monomers and oligomers and do not employ the same monomers and oligomers for each elastic modulus. As a result, adjusting the elastic module of this polymeric mixture cannot be accomplished simply by varying the relative amounts of monomers, oligomers, and crosslinks, as has been done with biomimetic substrates. [51]

Finally, the development of an innovative approach to multi-material 3D printing allows the creation of complex hybrid structures with advanced performance and functionality. This method uses highly extensible and UV-treatable hydrogel, along with various UV-curable polymers, including elastomers, rigid polymers, ABS-like polymers, shape memory polymers, and other (met)acrylate polymers. This innovation opens new possibilities for the design and manufacture of soft devices and machines with advanced functionality. The application of this technique is demonstrated in the creation of hydrogel-rigid compounds, 3D

printed meniscus with variable rigidity for wearable applications, 4D-printed cardiovascular stents with drug-release function, 3D printed ion conductors and deformation sensors with anti-dehydrating elastomeric layer. Fig. (2.11,2.12) shows DLP-based multi-material 3D printing. [52]

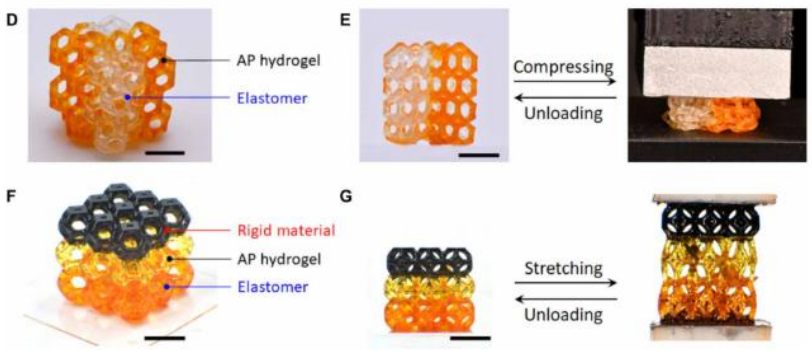

Fig. 2.11 (D to G) Schematics of the process of printing hydrogel-polymer multi-material structure. [52]

So, the multimaterial 3D printing of rigid polymer-reinforced hydrogel provides a promising solution to overcome some limits. To demonstrate this concept, a meniscus consisting of AP hydrogel (acrylamide-poly (ethylene glycol) diacrylate (PEGDA) reinforced by a rigid polymer is shown in Fig. 2.11. Despite the numerous benefits, 3D multi-material printing presents certain challenges such as materials compatibility which can't be easily combined because of their different adhesion and durability properties. Achieving high precision and resolution when using many materials can be challenging and further, the materials and equipment for 3D multimaterial printing can be expensive, limiting access to some applications. This is an important gap that should be filled in the future.

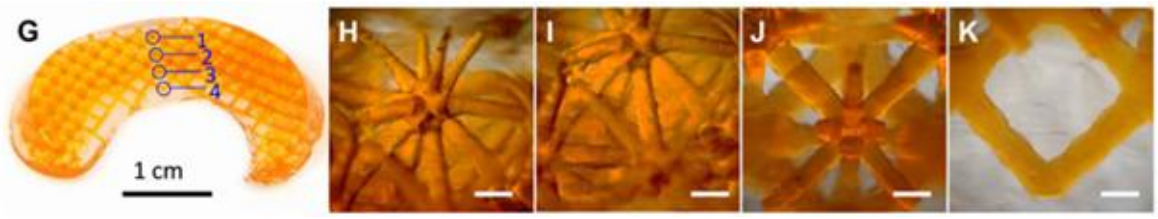

Fig. 2.12 (G) Snapshot of a printed meniscus made of hydrogel reinforced by rigid lattice structure. (H to K) The corresponding microscopic images of the microstructures at locations 1 to 4 within the printed meniscus, (H to J) Chemical structures of cross-linked AP hydrogel, AP hydrogel–(meth)acrylate polymer interface, and cross-linked (meth)acrylate polymer, respectively. R, R1, and R2 are the possible middle chains in (meth)acrylate polymer. [52]

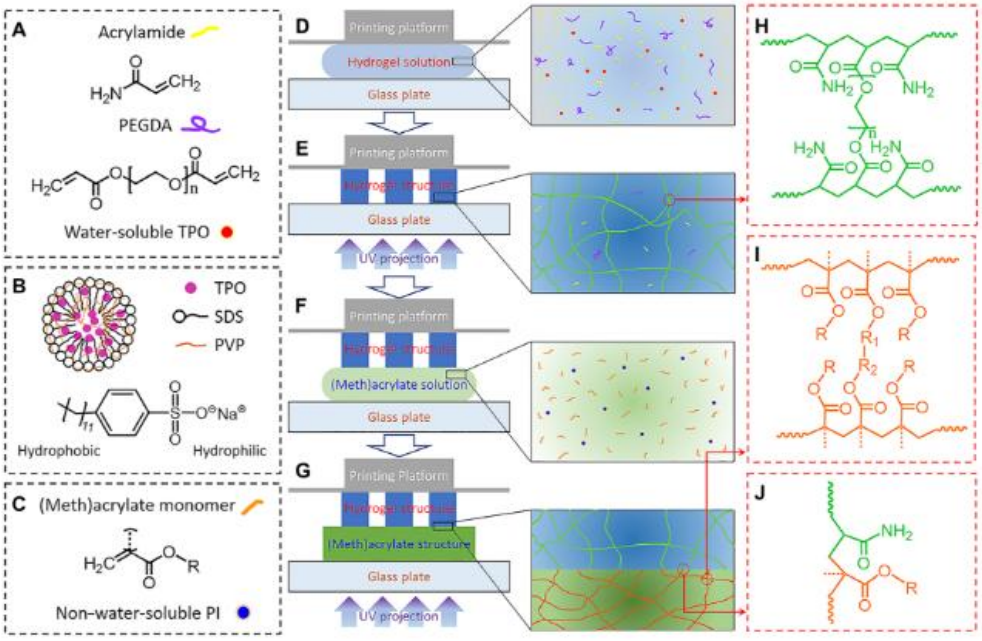

Figure 2.13 Materials and bonding mechanism. (A) Chemicals used to prepare the AP hydrogel solution. (B) Illustration of the water-soluble TPO nanoparticle. PVP, polyvinyl pyrrolidone. (C) Possible chemical structure of the (meth)acrylate-based polymer solution. PI, photo initiator. [52]

3. Materials and methods

This section discusses the materials and methods to fabricate the devices. This work investigated the production and characterization of an ink precursor-based sensor exploiting ionic conduction. A photopolymerizable monofunctional acrylate/acrylic acid resin with lithium chloride was used here. The absence of solvents leads to the prevention of water/solvent evaporation. In addition, transparency and adhesiveness are useful properties for biomedical applications: the former could make the sensors more aesthetic for everyday use, and the latter allows better integration with the human body. Before going into the details of materials and methods, we present a brief history of the various tests that led to the optimization of the components. This is followed by a presentation of the chosen materials.

3.1 Optimization formulation, Device manufacturing, and 3DLP

The study of the proposed thesis began with the search for the best formulation that could be easily printed and had all the features to present itself as a flexible conductive sensor. The initial research began with the PEGMEMA (Poly (ethylene glycol) methyl ether methacrylate**)** mono-functional acrylic macromer preparing different formulations with different percentages in weight of 1,2,5 wt% and various multifunctional crosslinks (Poly(ethylene glycol) diacrylate 250, Trimethylolpropane tri-acrylate, Trimethylolpropane tetra-acrylate, Trimethylolpropane esa-acrylate). Various molarities of LiCl salts were tested (0,5,1,1.5,2) and no substantial differences in conductivity were observed, only for a solubilization technique the chosen molarity was 1M. With these prepared formulations, simple casting procedures with a UV lamp and nitrogen were performed to evaluate the reticulation and then characterizations at the photo

reological level. The problems encountered were of a qualitative and practical nature: long reticulation times and too sticky samples, not ideal for subsequent mechanical-electric characterizations. The subsequent test envisaged the replacement of monofunctional crosslinkers with PEGMA (Poly (ethylene glycol) methacrylate), but this choice did not find a fast-printing process. The optimized formulation has a percentage of Acrylic Acid that has given the meeting point to the solubilization of the salt in the solvent-free resin, non-adhesive samples, and optimization of the printing parameters for even complex geometries. The 1 wt.% photoinitiator that gives cross-link value to the prepared formulation was an excellent choice for the printing process. The preparation of the resin and the subsequent characterizations will be presented in more detail in the following sections.

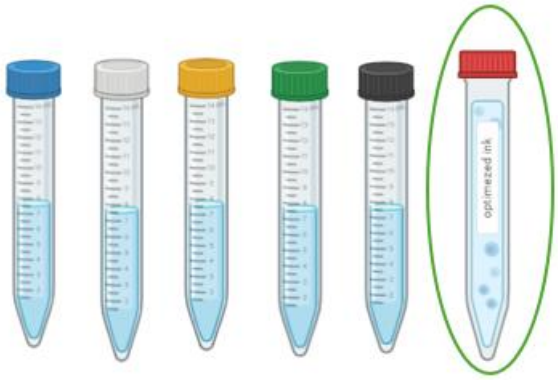

Fig. 3.1 Formulations tested as reported in the previous paragraph

3.1.1 Resin preparation

About the resin preparation, Poly (ethylene glycol) methyl ether methacrylate 300, acrylic acid, Bapo-Inimer, and methyl red dye were purchased from Sigma Aldrich (USA). Commercial lithium chloride salt was employed as conductive salt. The first step about the preparation of precursor ink was dissolving lithium chloride 1 M in PEGMEMA/acrylic acid solution under magnetic stirring (300 rpm, 15 min) at room temperature. In this way, the conductive component powder was

homogenously dispersed. Approximately 1 h later, a viscous transparent solution was achieved and then BAPO-INIMER and dye were added in the proper proportions and the entire solution was mixed at 300 rpm for 5 min. Methyl red (red color) is employed as a dye, to increase the printing resolution. A viscous homogeneous solution was prepared, consisting of 80% w/v of PEGMEMA and 20% w/v of Acrylic Acid. Subsequently, BAPO-INIMER, a crosslinking photoinitiator, was introduced into the formulation. This photoinitiator generates free radicals upon exposure to UV light. These radicals initiate polymerization, promoting the formation of chemical bonds between monomer molecules and consequently facilitating the creation of polymer networks. According to the literature, an effective amount of BAPO-INIMER required for the crosslinking of the precursor solution is approximately 1% w/v. The theoretical molar concentration tested for the precursor is 1 M. All necessary calculations, considering density and the desired volume, were carried out. In the literature, the ideal percentage of the Dimethyl Red dye is reported to be 0.1%, which is useful for the printing process to improve resolution (Fig. 3.5).

Follow a simple presentation about the precursor's ink. [53]

PEGMEMA

Poly(ethylene glycol) methyl ether methacrylate (PEGMEMA 300) is a versatile monomer belonging to the methacrylate family, characterized by the presence of a terminal methyl ether group. The structure of PEGMEMA is defined by the repetition of ethylene glycol units (denoted as n) and the presence of the methacrylate group, which allows the polymerization of the monomer. The terminal methyl group is less reactive than the hydroxyl groups, giving PEGMEMA greater chemical stability and reducing the likelihood of unwanted side reactions

during polymerization or application. This gives PEGMEMA several unique properties that make it suitable for multiple applications, particularly in biomedical fields such as biocompatibility useful for anti-fouling coatings such as medical device coatings, controlled drug delivery systems, and tissue engineering. PEGMEMA-based materials are used in biological and electrochemical sensors. Due to its transparency and compatibility with biological systems, PEGMEMA is ideal for applications in diagnostics and sensor technology. [54]

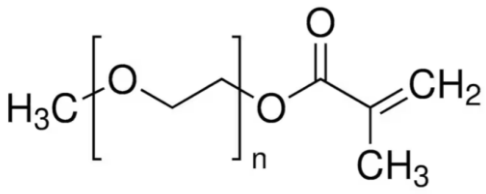

Fig. 3.2 Chemical formula of PEGMEMA [55]

Acrylic Acid

Acrylic acid is the simplest of the compounds containing a carboxylic group linked to a vinyl double bond. Acrylic acid is a very reactive molecule due to the presence of the carbon-carbon double bond and the carboxylic group. It is subject to polymerization and additional reactions. Being a carboxylic acid, it can donate a proton (H^+) and form acrylate salts and esters. The characteristics of acrylic acid (AAc) that are important for printing include its ability to polymerize quickly under UV light, its reactivity with other acrylic monomers during the printing process, and its ability to form covalent bonds to stabilize the ink structure. Additionally, AAc contributes to the formation of a chemical network which is essential to ensure the stability and mechanical strength of the printed material. The presence of AAc in the 3D printable structure contributes to its

capability and sensitivity to mechanical deformations, making it suitable for sensory applications. [56]

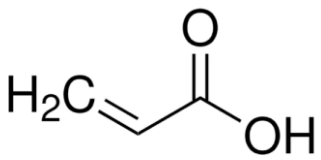

Fig. 3.3 Chemical formula of acrylic acid [57]

Bapo-Inimer

Phosphazenes (and polyphosphazenes) are composed of alternating nitrogen and phosphorus atoms, each with two substituents. The cyclic phosphazene trimer (hexachlorotriphosphazene) is an important small molecule model because its size allows for easier characterization with techniques such as NMR, X-ray diffraction, and weight measurement. These cyclic phosphazenes have similar bond angles and reactivities to polyphosphazenes, making them appropriate backbones for reactivity studies of multi-BAPO. Multi-BAPOs are compounds that contain more than one BAPO unit. The optimal amount of BAPO units necessary to print a stable structure with mono-acrylates was unknown until Jieping Wang produced BAPO cellulose nanocrystals, each containing roughly 2100 BAPO units. Inimers, or compounds with at least one initiator and one monomer unit (therefore presenting the role of photo initiator and crosslink) are also potential prospects for 3D printing applications. It was demonstrated that the BAPO-Inimer reacts with its acrylates both intermolecularly and intramolecularly, resulting in a crosslinked network. [54]

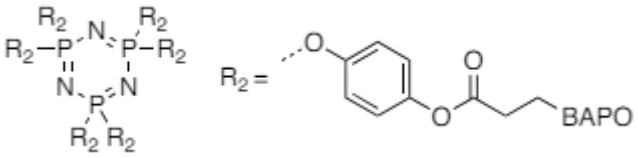

Fig. 3.4 Chemical formula of Bapo-Inimer. [54]

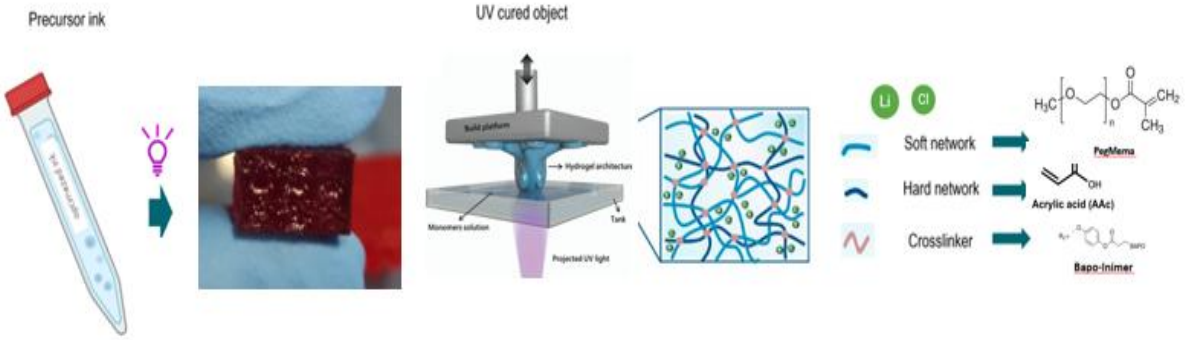

Fig. 3.5 Adapted from [58]

3.1.2 Rheology and Photo-rheology

Evaluating the rheological behavior of a polymer system provides insight into the material's response to deformation stress. A polymerizing system changes its physical state and mechanical properties, so the rheological response changes as polymerization progresses. Follow the development of mechanical and rheological properties as polymerization proceeds to provide information about the kinetics of the reaction. In particular, the behavior of elastic materials is described by Hooke's law (3), which represents the equation of line:

$\sigma = E \cdot \varepsilon$, where the deformation (ε) depends on the applied stress (σ), and these two terms are connected by the proportionality constant known as the "Young's modulus" or "elastic modulus" (E). This modulus provides information on the stiffness of the material and is identified by the slope of the line. Generally, the response of elastic materials, regardless of the intensity of the applied stress, follows a linear and reversible trend, meaning that all the mechanical energy supplied is absorbed and subsequently released when the stress ends, allowing the material to return to its initial shape. Afterward, the response starts to follow a non-linear and irreversible trend when a certain load, defined as the "yield point," is reached, and continuing to apply stress can eventually lead to the material's breaking point. The behavior of viscous materials, on the other hand, is described by Newton's law (Fig. 3.6), which also represents the equation: $\tau = \eta$, where the shear rate ($\dot{\gamma}$) depends on the applied shear stress (τ), and these two terms are correlated by the proportionality constant known as viscosity (η), which indicates the resistance opposed by the material to cracking. Specifically, viscous materials exhibit a linear and non-reversible response to applied pressure, so all the mechanical energy supplied is not absorbed but is dissipated as heat and friction. Finally, viscoelastic materials, which better represent reality, display an intermediate behavior between the two previously mentioned.

Specifically, the deformation obtained after the application of stress can be given by the sum of the elastic and viscous components. Therefore, the viscoelastic regime can be achieved when there is proportionality between the applied load and the obtained deformation, and this can be described with mathematical models obtained by combining Hooke's equation and Newton's equation. In fact, the rheometer is used to apply sinusoidal shear stress $(\tau(t) = \tau_0 \sin(\omega t)$ and measure the sample's reaction in deformation. The function will always be a sinusoid, $(\gamma(t) = \gamma_0 \sin(\omega t - \delta)$, with the factor δ delayed relative to the input. From the ratio between τ(t) and γ(t) it is possible to obtain the dynamic modulus G which is a complex number divisible in:

$$G = G' + iG'' = \frac{\tau_0}{\gamma_0} cos\delta + i \cdot \frac{\tau_0}{\gamma_0} sin\delta$$

Figure 3.6

where G' = $\frac{\tau 0}{\gamma 0} \cos \delta$ is the storage shear modulus (a measure of energy stored and recovered per each cycle) and G'' = $\frac{\sigma 0}{\tau 0} \sin \delta$ is the loss modulus (a measure of the energy dissipated by the internal frictions). From the mechanical point of view, G' represents a measure of the stiffness of the sample. [30] The rheometer can be fitted with a UV lamp to analyze the kinetics of photopolymerization. The mechanical properties (G', G'') are measured to determine photo-reactivity. In general, when the material is in the liquid-viscous phase, such as monomeric formulations, the viscous modulus is higher than the elastic modulus, when the material is solid, because of cross-linking, the elastic modulus becomes higher. In the curve obtained from the test, if one has cross-linking of the formulation, one should observe the growth of both modulus values, but above all also a reversal point where the elastic modulus exceeds the viscous modulus: this point

is called the gel point. The gel point is particularly important for a 3D printing process. [59]

In this work, a rheometer was used to evaluate the crossover time of the studied material through photorheological tests. The tests were conducted with an Anton Paar rheometer (Physica MCR 302) in a flat-flat configuration, the upper part of which had a diameter of 25 mm, and a UV lamp (Hamamatsu LC8). For the lower plate of the rheometer, a quartz plate was used to be transparent to the UV beam incident. The tests were performed at a temperature of 25°C, with an interval of 200 micrometers between the plate and the glass plate on which the formulation was placed. Initially, the material was subjected to amplitude tests to identify the linear viscoelastic range (LVR), where the storage modulus (G') and loss modulus (G'') are stable. From the amplitude test, it was possible to choose an amplitude value (10%) to be applied later. Next, photo rheology tests were performed at a constant frequency of 1 Hz and a voltage value of 10% taken from the previous amplitude tests, allowing the evaluation of the formulation crossover time by observing the variation of G' and G'' over time. The test begins by placing the formulation on the glass slide and then starting the mechanical activation; after 60 seconds, the UV lamp is turned on and kept running until the end of the test.

Figure 3.7 Tools Used

3.1.3 % Gel

The gel percentage test (% gel) was used to determine the resin's insoluble fraction as well as the amount of unreacted pre-polymer and photoinitiator residues in the samples. This is a critical feature since photoinitiator or polymer fragment residues might cause instability, toxicity, or incompatibility, particularly when in contact with biological materials. To perform the test, a polymer sample is subjected to crosslinking, and its initial weight (w0) is measured. The sample is then immersed in a chloroform solution for 24 hours and kept in a net to prevent any fragments from spreading. During this process, the non-crosslinked components dissolve into the solvent. After immersion, the sample is dried for another 24 hours to remove any remaining solvent, and its final weight (wf) is measured. To ensure more accurate measurements, the weight of the net is recorded before the treatment. Subsequently, the sample is weighed with the net, and the net's weight is subtracted to obtain only the weight of the sample. By comparing the initial weight with the final dried weight, it is possible to calculate the percentage of crosslinked polymer relative to the total mass of the sample. The formula for calculating the gel percentage is:

$$\%\text{Gel} = \frac{wf}{w0} * 100$$

A higher gel percentage indicates a greater level of crosslinking, meaning that a larger portion of the polymer has formed an insoluble network. Conversely, a lower gel percentage suggests less crosslinking, and a larger amount of unreacted polymer still present in the sample (Fig. 3.8).

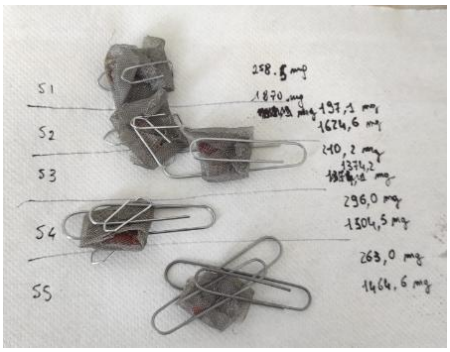

Figure 3.8 % Gel method. Preparation Sensor in chloroform, then Drying process of samples

3.1.4 3D_DLP Printing

The Asiga MAX UVX27 printer, manufactured by Asiga, was used for the 3D printing phase. It's a DLP-type printer with an LED light source emitting at a wavelength of 385 nm, a spatial resolution of 50 µm, and a z-axis axis of 1 µm. This printer can be controlled via a program, Asiga Composer, supplied by Asiga. Through this program, files of the objects to be produced are sent to the printer, with different 3D models designed using SolidWorks CAD software, converted into STL file formats, and 3D–printed. The process of obtaining each layer is based on the vertical movement of the platform on which the sample is printed upside down; in the first step, the platform approaches the bottom of the tray (approach step), in which the selected formulation has been placed until it leaves a space equal to the thickness of the layer to be cross-linked; at this point, the LED light is switched on and irradiates the formulation for the set time (irradiation phase), then the platform moves away from the tray (removal phase) allowing the formation of a continuous layer of liquid formulation, before the subsequent approach. The main parameters that were varied during the printing process are layer thickness, light intensity, and irradiation time. On specific occasions, the speed of movement of the platform during approach can be changed to limit the formation of bubbles within the formulation, which could have caused defects in the printed samples. It is possible to group the different

layers into several sections (ranges) and change the printing parameters from one range to the other. Generally, each object is produced by differentiating at least the parameters of the first printed layers, from the rest. These initial layers are usually made with higher irradiation times or intensity higher, to promote adhesion of the cross-linked material to the platform (so-called burn-in layers).

Fig. 3.9 Asiga MAX UVX27 printer. [60]

Several geometries have been printed as can be seen from the inserted CAD shown in Fig. 3.10 A thickness of 20 µm was used for the Burn-in layers and for subsequent layers 50 µm with a light intensity of 35 mW/cm2 with times of 20 s. The heater temperature of the printer was set to 40 °C for the entire process. The vat surface was wetted with silicone oil to optimize printing, to avoid the adhesion of the photocured methacrylates while printing, and to make the sample non-spotty and pickable. The post-curing procedure provided that the printed objects were washed with ethanol for 5 min to remove any residues of unpolymerized resin subjected to sonication and finally were irradiated with UV light with Asiga Flash, post-cure unit for another 5 min for both sides of the sample.

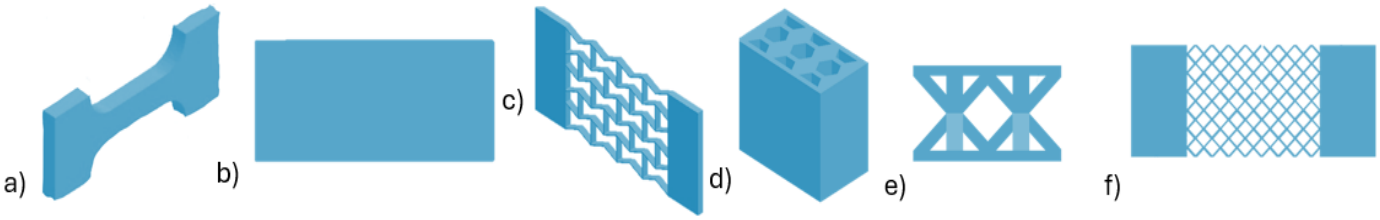

Figure 3.10 CAD for printing: a) Dogbone, b) Bulk, c) Re-entrant, d) Honeycomb, e) Stars, f) Mesh

3.2 Sensor characterization

To run tests with different parameters, various configurations matching the features of the machines were designed. Kapton-copper electrodes were employed to construct sensors. Bulk and honeycomb models were utilized to analyze compression performance. Additionally, dog bone-shaped samples and mesh geometry were fabricated to evaluate the tensile properties under different conditions. These diverse configurations allowed for a comprehensive analysis of sensor performance and material behavior under various mechanical stresses.

3.2.1 Tensile Test

Tensile tests were carried out to assess the mechanical properties of the improved sensor. As previously described in sensor fabrication, DLP methods were used to create a dog bone and mesh of solvent-free light-cured resin. These tests were performed using a Z5 tensile machine with a 500 N load cell. Two knurled clamps were used to grab the sample edges. Trial settings and data storage were carried out using THSD software. Four examples of each material were tested to the point of rupture. One of the machine's two clamps is fixed. The other is movable: a linear motor lifts it up, stretching the sample. The load cell installed on the moving clamp measures the force applied. The stress value (σ) is calculated using the formula σ = F/A, where F is the measured force and A

is the sample's cross-sectional area, which can be manually modified using the software. At the same time, strain is measured based on the linear motor's location. The software calculates the strain (ϵ) using the formula $\epsilon = (l - l_0)/l_0$, where l equals the current length of the sample, determined by the position of the motor, and l0 is the length of the sample at rest. The slope of the straight line in the first linear section of the graph reflected the young modulus or elastic modulus. The average values and standard deviations of these parameters were then computed, which represented the mechanical behavior of the material and allowed the sensor's performance to be displayed (Fig. 3.11).

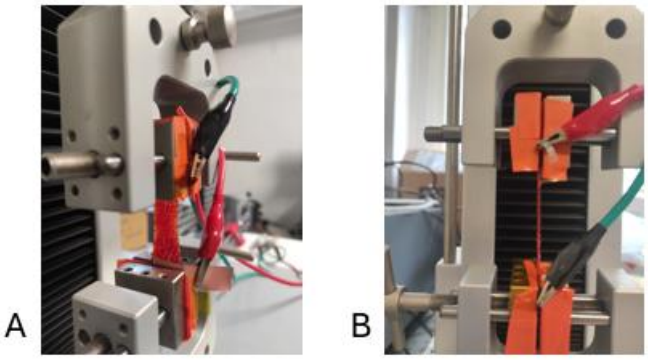

Figure 3.11 Tensile test. A) Tensile test setup, and B) Extension of a sample during a tensile test

3.2.2 Electrical characterization

An LCR meter (BK Precision 894) was used to investigate the variation of electrical characteristics during external strain. LabView (National Instruments) was used to set up parameters and gather data. The full test bench is illustrated in the figure (Fig. 3.12). A parallel between a resistance and a capacitor (Rp and Cp, shown in Figure) was employed as an impedance model. Stimulation frequencies of both 20 Hz, 50 Hz, and 1000 Hz were applied, and the signal voltage amplitudes studied are 20 mV,50 mV, and 0.5 V. Electrical characterization was useful to determine the best sensitivity to external voltage, and the stability of the sensor

and to understand which of the parameters (Rp or Cp) and at what frequency was best to work. The different experiments conducted enabled the optimization of the frequency and voltage levels of 1000 Hz and 0.5 V. Cyclical acquisitions (20 cycles at 40% strain) were performed to examine measurement repeatability and durability tests were performed every 7 days for 35 days to ensure that mechanical and electrical characteristics didn't deteriorate. (Fig. 3.12)

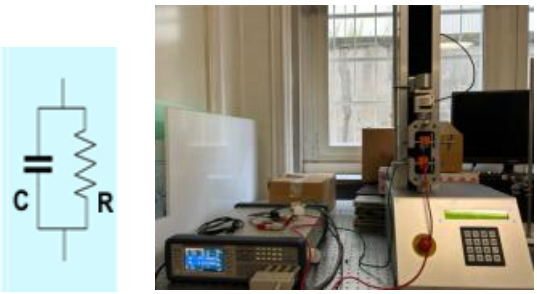

Figure 3.12 Modelling impedance as a resistor parallel to a capacitor and Tools used

3.2.3 Compression Test

First, small samples (bulk/honeycomb with the same dimensions) were used to evaluate the electrical-mechanical response of the sensor under compression. Dynamic compression tests were performed with the Tensile Test Z5 500 N machine and controlled through the THSSD program with a 1mm/min velocity, a displacement slightly less than the sample thickness, a load of 100 N, and a pre-load of 0.05 N. The compression test was carried out by applying homogeneous pressure to the surface of the sensors using a dedicated loading platform, allowing the delivered force to be carefully measured and controlled. During each test, changes in the sensors' electrical characteristics, such as strain response and sensitivity, were recorded. Each test setup was repeated to confirm that the results were consistent, and the collected data was statistically evaluated to assess the sensor's resistance to compression under various

simulated use situations. Static compression test trials were performed by applying different weights (20, 100, 200, 500 mg) on the top surface of printed sensors (area of 10 × 10 mm^2). A pre-load of 1 g was used to allow good electrical contact with the electrodes. As for the static compression tests, an electrical measurement of 30 s with 1000 Hz and 0,5 V was performed for each weight. All the tests were performed by calculating the single pressure on the sample.

3.2.4 Temperature Test

The dependency of electrical characteristics on temperature has been investigated further. The sensor was placed in the oven while Rp and Cp were measured using the LCR meter. The temperature ranged from room temperature (25°C) to 60°C in 5°C increments, with 1-minute static acquisitions between each temperature step. All research employed an electrical stimulation frequency of 1000 Hz. Three samples were evaluated in this manner to provide more reliable statistical data. Subsequently, the samples were cooled down to room temperature, and the resistance was measured again across the same temperature range (Fig. 3.13).

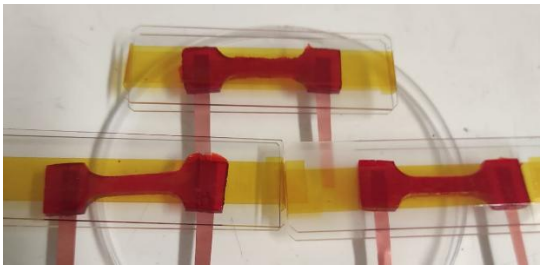

Figure 3.13 Preparation sample for temperature test

4. Results

4.1 Gel characterization

4.1.1 Photoreology

A detailed analysis was conducted to determine the photocurable resin's reactivity and mechanical properties, with a focus on its stress performance. Initially, an amplitude sweep test was performed on unpolymerized solutions to determine the linear viscoelastic range (LVR) in which the storage modulus (G') and loss modulus (G'') remain constant. An ideal strain of 10% was identified, which served as the baseline for subsequent experiments and demonstrated the gel's capability to maintain mechanical integrity when deformed. The photo rheology analysis used a 10% constant strain with an oscillation frequency of 1 Hz. After 80 seconds of UV light exposure, the crosslinking process began. The gelation point is seen when the storage modulus (G') exceeds the loss modulus (G''), indicating a change from a liquid to a three-dimensional solid structure (Fig. 4.2). The viscosity of this resin was investigated in response to the shear rate, showing pseudoplastic (shear-thinning) behavior Viscosity decreased as the shear rate increased, allowing the material to move more easily (Fig. 4.1). This feature makes the resin ideal for 3D printing applications requiring homogeneous deposition and high-detail precision. The resin’s properties result from the synergistic interaction of its components. PEGMEMA contributes elasticity and flexibility, acrylic acid enhances strength and adhesion, while the BAPO-inimer photo initiator ensures fast UV-induced polymerization. Lithium chloride further introduces ionic conductivity, making the resin an excellent choice for complex structures and advanced printing technologies.

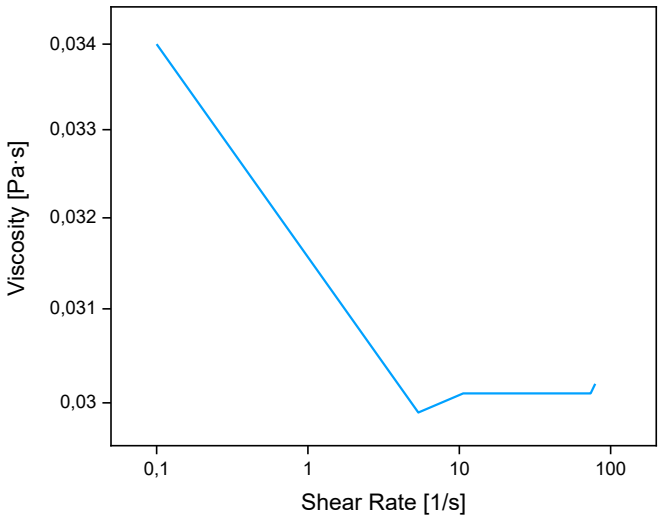

Fig. 4.1 Viscosity of formulation under continuous shear rate sweep

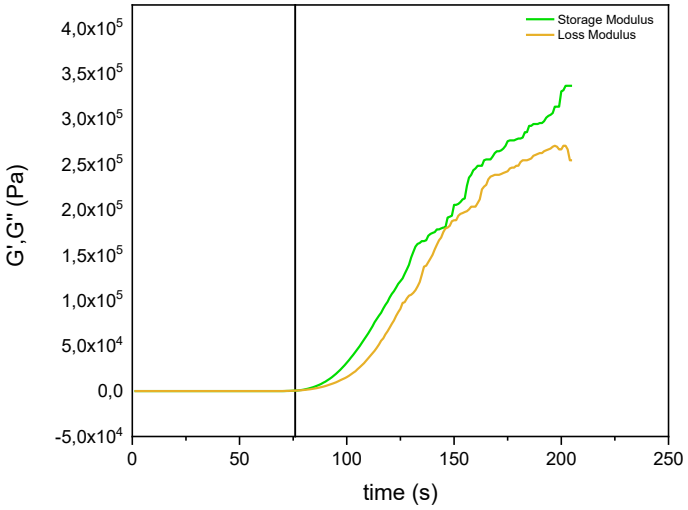

Fig. 4.2 Real-time photorheological measure of the formulation, after 80 s start UV

4.1.2 %Gel

Two formulations were examined to assess the gel content: one with 20 wt% PEGMA and the other with 20 wt% acrylic acid. Five samples from each formulation were tested. Acrylic Acid formulation demonstrated gel content levels of approximately 70%, instead with the formulation with PEGMA, an average value of 80% was obtained, indicating a substantial degree of crosslinking and efficient polymerization. These results suggest that the unpolymerized fraction is minimal, even considering the significant salt content in the composition. A high gel content highlights the formation of a well-structured and stable hydrogel network, which is essential for applications requiring durable, resilient inks with excellent printability (Fig. 4.3, 4.4).

Sample Acrylic Acid	**Initial Weight Sample (mg)**	**Final Weight Sample (mg)**	**% Gel (%)**
Sample 1	258,5	159,3	61,6
Sample 2	197,1	151,9	77,1
Sample 3	210,2	139,2	66,2
Sample 4	296,1	197,1	66,5
Sample 5	263,1	171,4	65,1

Fig. 4.3 Table of %Gel results in samples with Acrylic Acid

Sample PEGMA	**Initial Weight Sample (mg)**	**Final Weight Sample (mg)**	**% Gel (%)**
Sample 1	234,3	198.6	84,8
Sample 2	257,3	212,9	82,7
Sample 3	232,6	191,7	82,4
Sample 4	233,3	159,2	68,2
Sample 5	294,9	242,7	82,3

Fig. 4.4 Table of %Gel results in samples with PEGMA

4.2 Device performances

The samples obtained from the printing process and on which all the relevant characterizations have been made are shown in Figure 4.5.

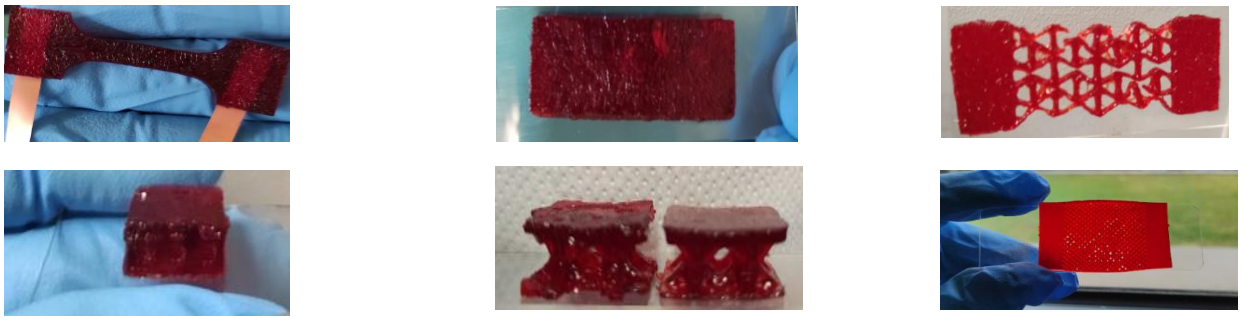

Figure 4.5 CAD for printing Dog bone, Bulk, Re-entrant, Honeycomb, Stars, Mesh

4.2.1 Tensile, Compression, and Electrical Tests

Compression and tensile tests were conducted. Particularly, tensile tests up to failure, durability tests, and hysteresis tests were performed on dog bone and mesh samples. Mechanical-electrical analyses demonstrated the importance of material selection and sensor configuration to ensure optimal performance. Copper electrodes provided accurate and stable measurements, while tensile tests revealed increased electrical resistance due to the elongation of the material, which induced an increase of conductive path. The sample shows a linear response to applied strain.

Optimization at 1 M was carried out by testing different molarities on cross-linked samples by casting and evaluating the stability of the resistance over time. Tests were carried out for molarity 0.20,0.40,0.60,0.80 M LiCl. The data were too noisy and not evaluable (the order of resistance was MΩ). Furthermore, various molarities (0.5, 1, 1.5, and 2 M) were tested without observing significant differences in conductivity. Consequently, a molarity of 1 M was chosen for a

specific solubilization technique. The sample showed good stretchability, with elongations more than twice the initial length, and a low Young's modulus, indicative of high flexibility. The stress-strain curves confirmed the behaviour typical of elastomers, with a gradual increase in stress up to about 2.5 MPa before sudden breaking. In the tensile tests until failure, Young's modulus (Fig. 4.8) was computed in the graph as the slope of the linear region in the stress-strain curve (Fig. 4.6, 4.7) Compression and tensile tests (Fig. 4.9) conducted on samples with different geometries made it possible to assess the sensitivity and behaviour of the material under stress. From the ΔR/R-ϵ curves, a constant sensitivity value, defined as the slope of the curve, was obtained over time, indicating the relationship between the relative variation in resistance (ΔR/R) and strain (ϵ) across the measured range. Durability tests were performed on the samples with a maximum deformation of 40%, monitoring the sensitivity and Young's modulus over time. The samples were kept under ambient conditions and stored in plates with Parafilm for a total period of 35 days (Fig. 4.8). During the test, minimal variations in the measured parameters were observed, mainly attributable to environmental fluctuations in temperature and humidity.

Furthermore, the hysteresis test confirmed good structural stability over 10 cycles, with cyclic deformations of 40% of the initial length, which is essential for long-term reliability. Studying the hysteresis curve (Fig. 4.10, A) is crucial to understanding material behaviour, improving design, and predicting performance. The deformation response of the material underloading and unloading does not follow the same path, generating a closed curve, the area of which represents energy dissipation. The viscoelastic behaviour of the material is evident, with deformation dependent on time and applied load. A progressive shift in the hysteresis curve is observed in the sample, indicating a reduction in deformation resistance over time, probably due to relaxation of the polymer

matrix. During the hysteresis test, the impedance of the material was also measured. Electrical resistance (Fig. 4.10, B) showed a decreasing trend, reflecting a reduction in internal resistance due to viscoelastic relaxation. In addition, the material was also sensitive to changes in capacitance, suggesting that capacitance may be an effective parameter for strain monitoring.

Compression tests on PEGMEMA sensors with a crosslinker and 1 M salt showed the influence of geometry on mechanical and electrical resistance, comparing two configurations: bulk, solid and uniform, and honeycomb, lighter and more structured. During compression, electrical resistance decreased in both configurations, with differences in sensitivity and linearity of the response. The honeycomb structure exhibited greater sensitivity, with a more pronounced change in resistance, while the bulk geometry showed a more gradual response and lower deformability. (Fig. 4.12,4.13) These results demonstrate how the choice of geometry is critical to optimizing sensor performance according to the specific application, balancing sensitivity, linearity, and mechanical strength. The capacity trend in relation to compressive strain is also shown for possible future developments on the capacity study (Fig. 4.14).

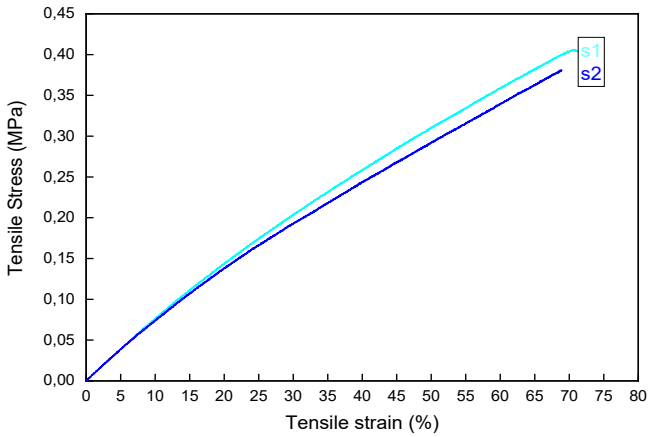

Fig. 4.6 Tensile stress-strain curves, dog-bone

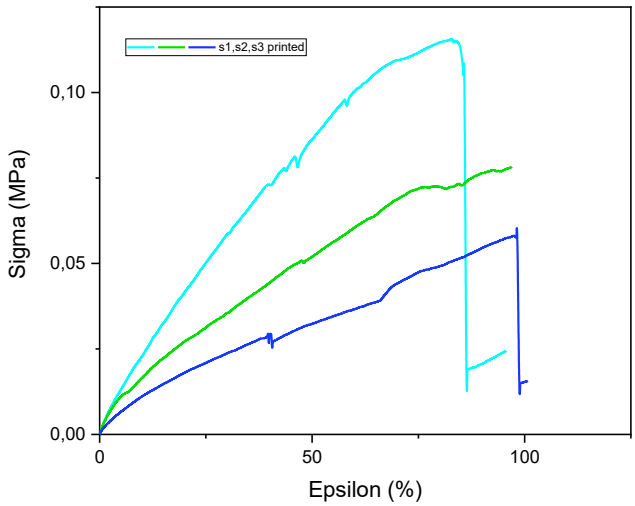

Fig. 4.7 Tensile stress-strain curves up to rupture of the dog-bone samples

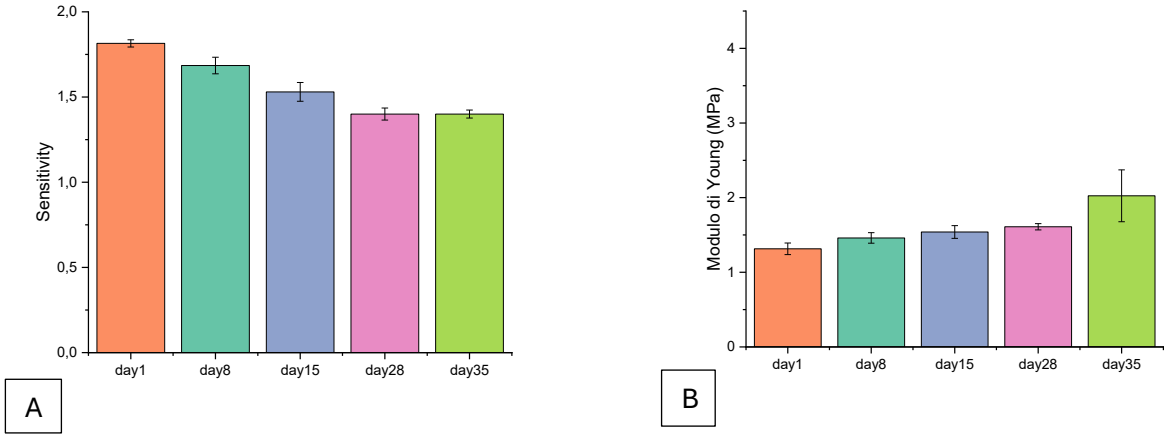

Fig. 4.8 Strain sensitivity (A) and Young's modulus values (B) measured over different days, dog-bone samples

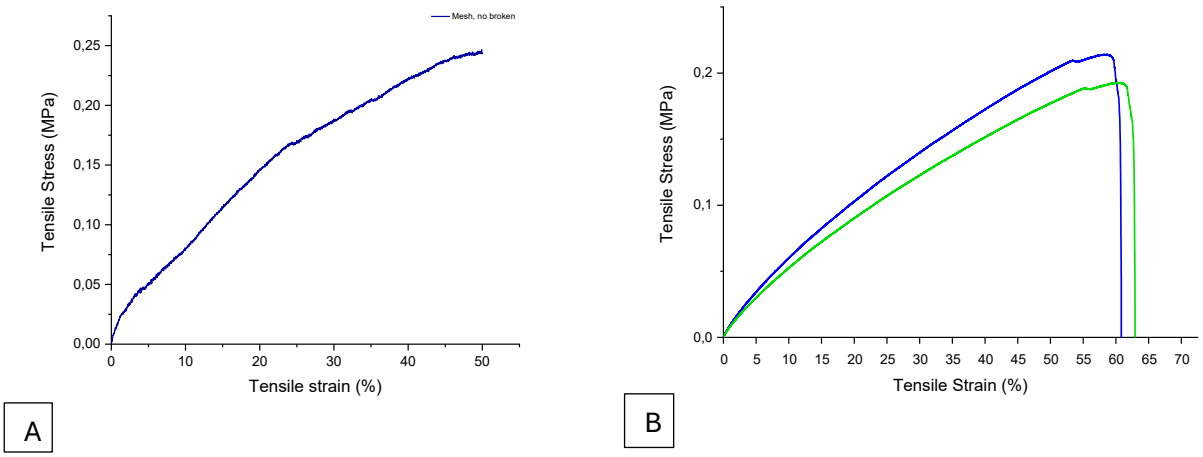

Fig. 4.9 Stress-strain curve for mesh sample no broken (A), (B) broken sample

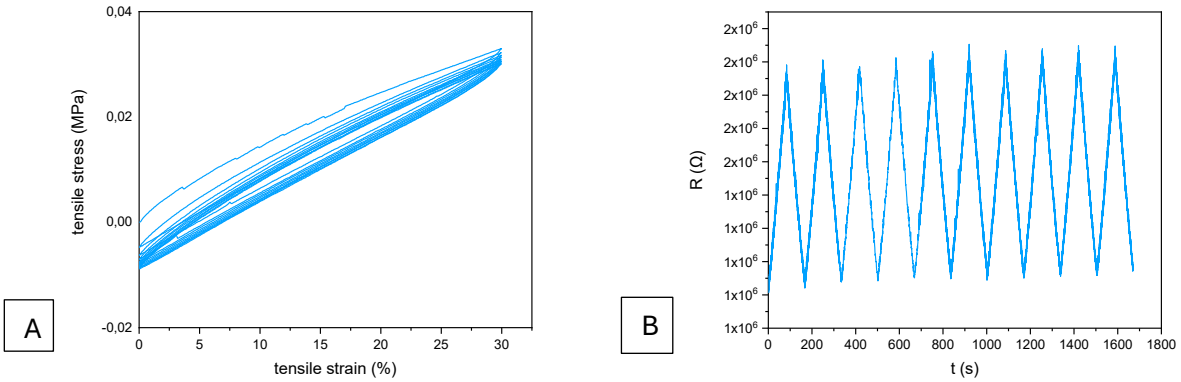

Fig. 4.10 Stress-strain curve (A), resistance performance over time (B), dog-bone sample

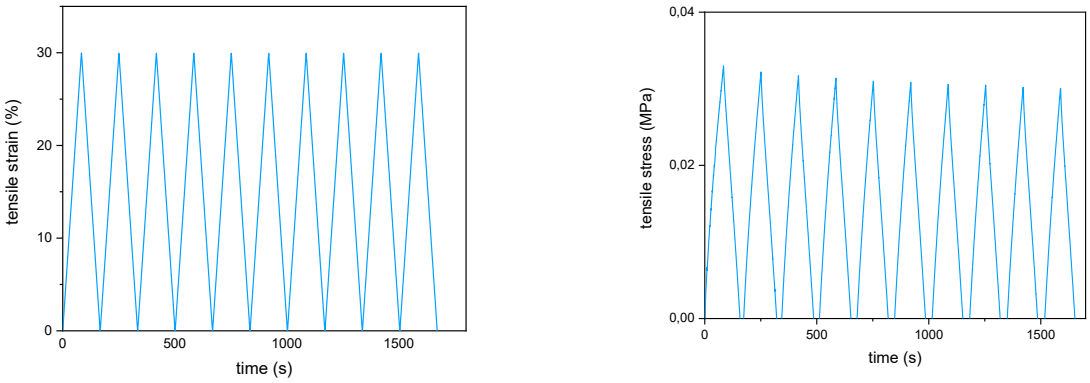

Fig. 4.11 Hysteresis cycle, tensile stress, and strain over time, dog-bone sample

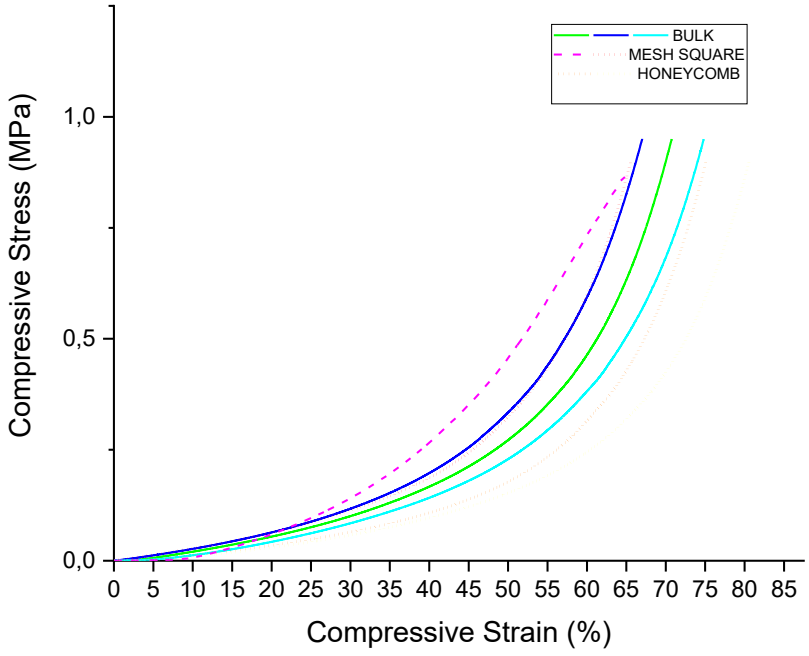

Fig. 4. 12 Compressive stress-strain curves, bulk-mesh square-honeycomb

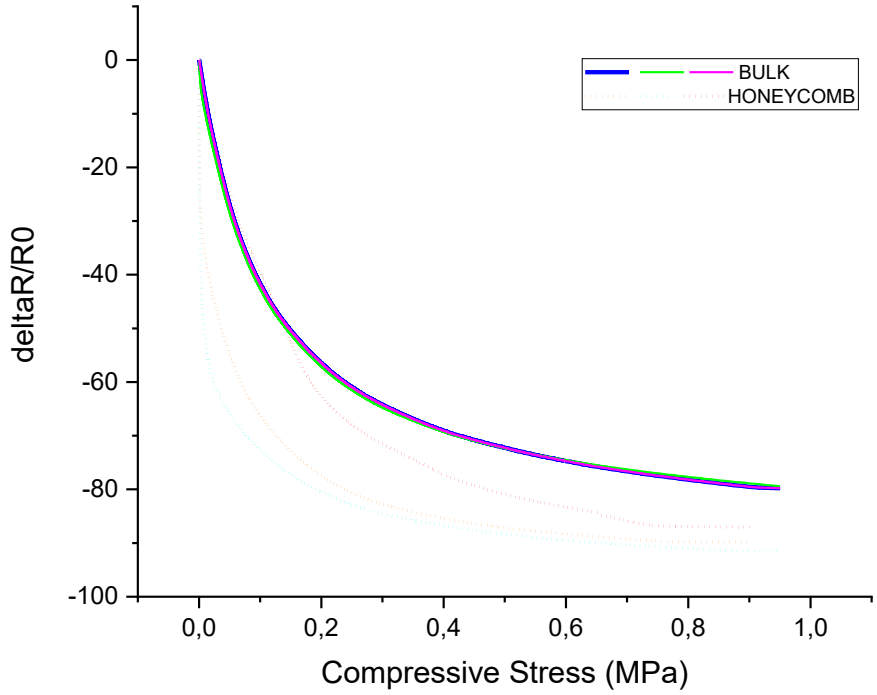

Fig. 4.13 ΔR/R-σ compression curves, bulk,honeycomb

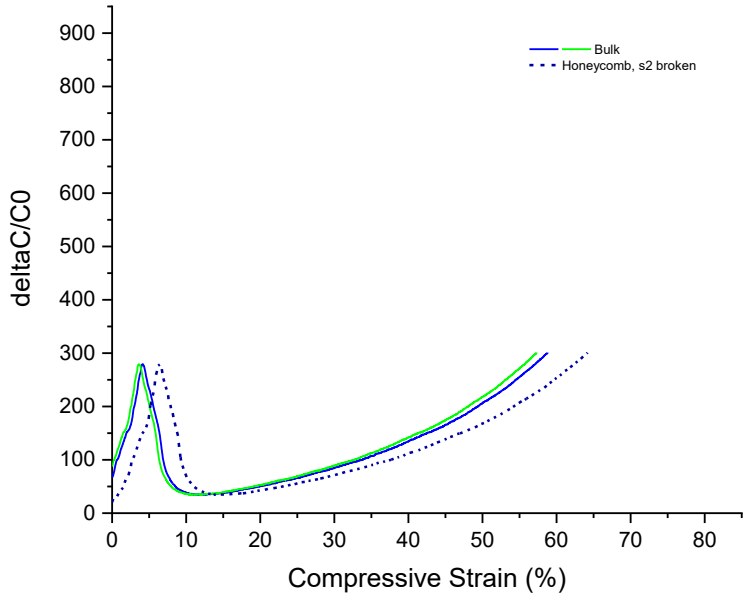

Fig. 4.14 Compressive strain/Capacity variation, bulk-honeycomb

4.2.2 Temperature dependency of resistance

To perform a more targeted study on the effect of temperature on material resistance, samples were placed in a constant humidity oven and gradually increased in temperature. Resistance was measured at 5°C intervals using an LCR meter connected to the sample electrodes, allowing a curve to be constructed by interpolating the gathered data. The temperature dependence showed the device's particular thermal behavior: the resistance Rp lowers as temperature increases up to a threshold of 50°C. These phenomena are linked to increased Li+ ion mobility, which is helped by lower polymer viscosity and higher heat energy, which improve ionic conductivity. However, once beyond 50°C, a switch takes place that shows an increase in resistance. To analyze this change, measurements on the samples were performed after a three-hour cooling time, but the resistance trend remained constant. It was proposed that this increase in resistance is caused by events such as glass transition, crystallization, or thermal deterioration of the polymer or photo initiator. These alterations influence ionic mobility and, in some situations, may modify the solubility or recrystallization of LiCl, reducing the availability of mobile ions. These results highlight a key limitation of the devices: temperature and strain both have an interdependent effect on the electrical parameters (Rp and Cp), making it impossible to separate their contributions if both stimuli are unknown. As a result, for appropriate use, the sensors must function at a constant temperature for strain detection or vice versa. In this context, additional DSC (Differential Scanning Calorimetry) research was undertaken. It’s a technique for studying material thermal transitions. There are two curves, the first (in black) and the second (in red), representing the sample's first and second thermal scans, respectively. In the first run, there is a clear transition of about 60°C,

shown by a peak in the heat flow, which could be due to a melting event or a glass transition. The second run exhibits a more regular pattern with no such obvious transition, implying that the material has undergone an irreversible change, such as the loss of a crystalline organization or the end of a stabilization process. Finally, to confirm the sensor's potential application as a temperature detector, additional research, such as TGA and spectroscopic investigations, would be required to determine the underlying mechanisms causing the observed changes. These evaluations could help in optimizing sensor design for certain application conditions, resulting in more consistent and predictable performance (Fig. 4.15, 4.16).

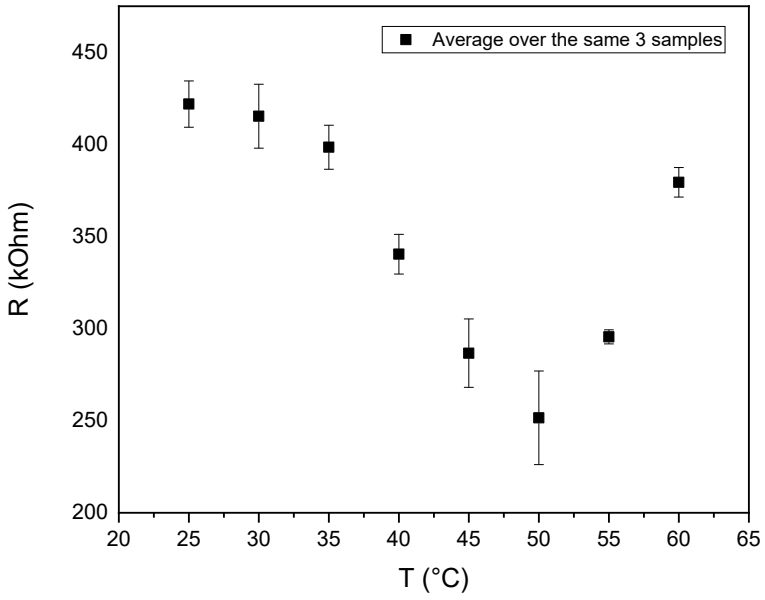

Fig. 4.15 Variation of resistance during the temperature test

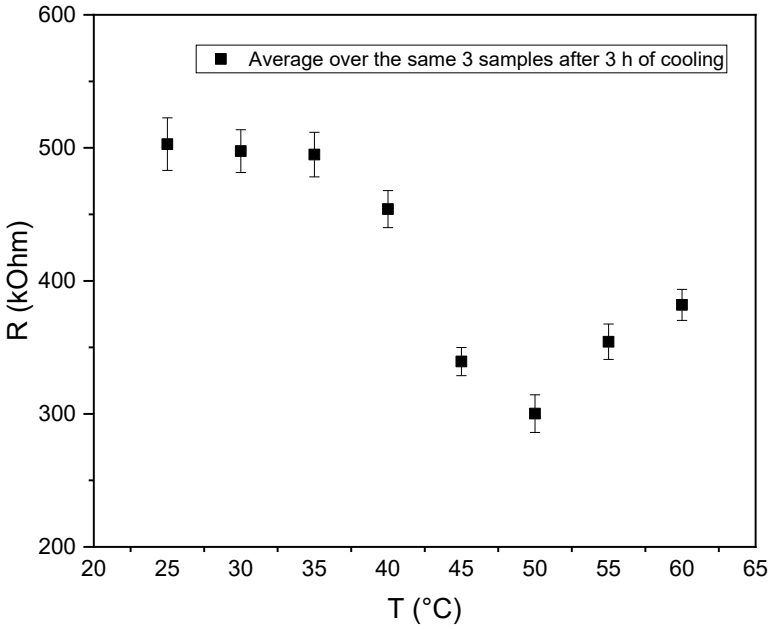

Fig. 4.16 Variation of resistance during the temperature test post-cooling

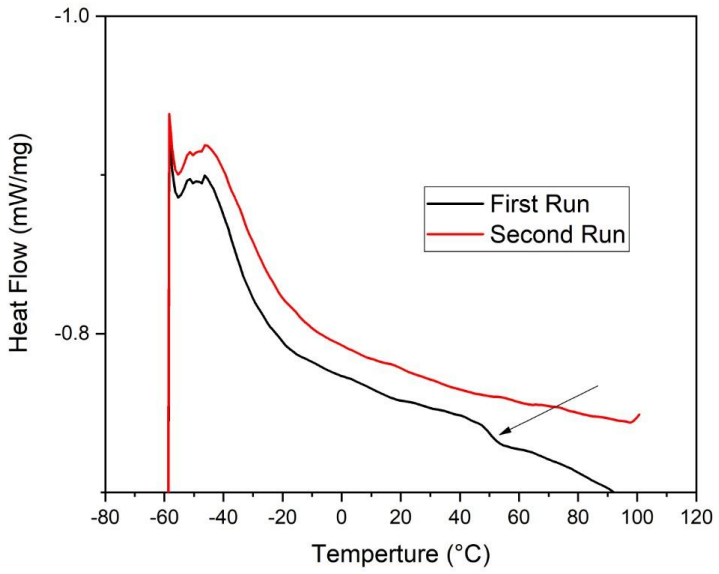

Figure 4.17 Differential Scanning Calorimetry

4.2.3 Applications

To conclude the study, vivo tests were conducted using the developed sensors on various body parts to evaluate the impact of deformation on the measured resistance. Vocal cord vibration and heartbeat measurements were also performed, but the results found were too noisy and difficult to represent. The following images illustrate the results obtained (Fig. 4.17, 4.18).

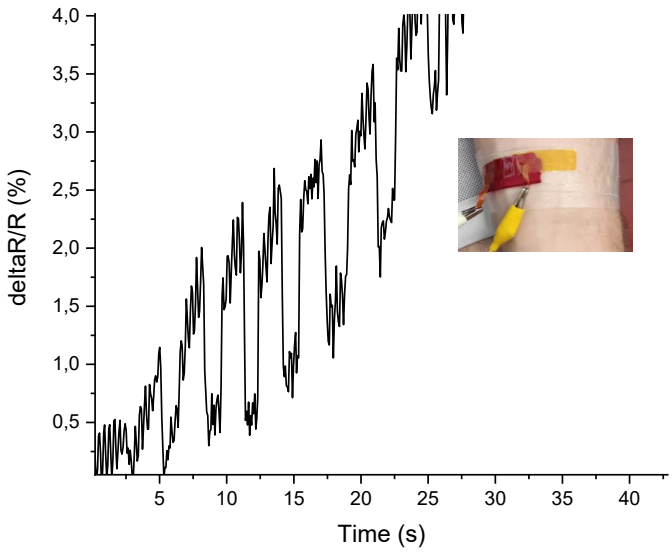

Fig. 4.17 Forearm muscle bending

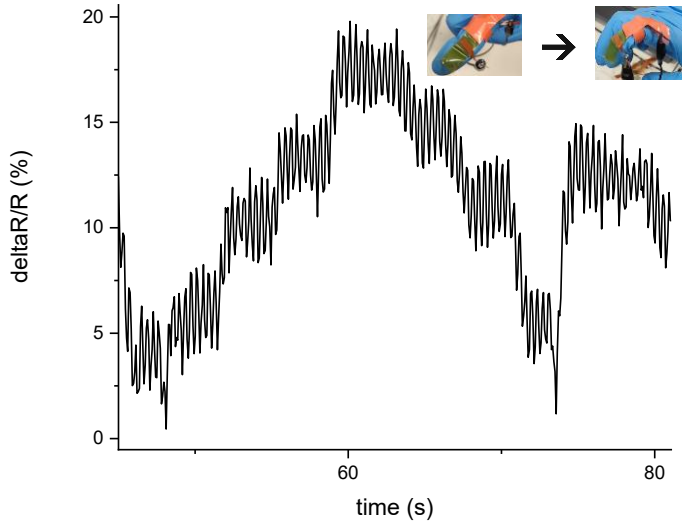

Fig. 4.18 Finger bending monitoring – Resistance and capacitance signal in reaction to different bending angles

Conclusions

In recent years, the development of flexible sensors has grown rapidly driven by emerging needs for wearable devices in various fields such as medical, robotics, and human-machine interaction. Advanced polymeric materials with flexibility, mechanical strength, and electrical qualities are becoming increasingly important for developing sensors that may be easily integrated into everyday life or medical devices. Among these new materials, poly(ethylene glycol) methyl ether methacrylate (PEGMEMA) combined with acrylic acid and lithium chloride (LiCl) has demonstrated significant promise as a base for developing low-cost, stable, and easy-to-manufacture sensors using 3D printing processes. The developed sensor is made from a photopolymerizable resin that includes PEGMEMA as the main polymeric matrix, acrylic acid to aid in the polymerization process, and lithium chloride, which works as a conductive component, allowing ionic conduction within the sensor. One of the formulation's important new features is the absence of solvents and aqueous components, which improves the resin's stability and minimizes its sensitivity to environmental fluctuations like humidity. This element leads to more reliable sensors working even in less regulated conditions. The resin composition was optimized with the addition of acrylic acid, which successfully solubilized lithium chloride within the matrix, minimizing unsuitable adhesion issues and easing the 3D printing process, even for complex geometries. This process was critical to obtaining sensor samples suitable for future applications. The sensor's maximum deformation is 80%, making it perfect for monitoring complex movements. It has a sensitivity of 1.8 and a Young's modulus of 1.3 MPa, indicating a high capacity to detect deformations while maintaining structural integrity. Mechanical testing revealed remarkable elasticity, with the sensor remaining intact even under extreme stress, demonstrating the complete integration of lithium chloride into

the polymeric matrix. Furthermore, the gauge factor of about 1.8 supports its efficacy in detecting strain fluctuations, making it excellent for applications like muscle motion detection. In terms of durability, the sensor performed well under multiple cycles of stress and release, showing no signs of degradation after ten cycles, both mechanically and electrically. From an electrical standpoint, lithium chloride played an essential role in ensuring efficient ionic conduction within the polymer matrix. One significant advantage of this formulation is its electrical stability, even under varying environmental conditions. In many applications, the sensitivity of conductive materials to humidity and temperature can lead to signal instability. However, the solvent-free formulation of this sensor significantly reduced such issues, ensuring reliable electrical responses across different environmental conditions.

During the temperature tests, the sensor maintained stable electrical resistance over a wide temperature range, thanks to lithium chloride, which preserved ionic conductivity even under thermal fluctuations. This aspect makes the sensor particularly suitable for real-world applications where temperature fluctuations are frequent, such as in medical devices or outdoor use. The PEGMEMA-based sensor was tested for its applications in wearable technology, particularly in health monitoring. The tests demonstrated that the sensor could accurately detect physiological signals, such as muscle contractions and joint movements, with a high degree of precision. Thanks to its flexibility, the sensor perfectly conforms to the body surface, providing real-time data without causing discomfort to the user. This makes it ideal for integration into wearable devices designed for monitoring physiological parameters. To conclude, the sensor combines excellent mechanical stability, reliable ionic conductivity, and stable resistance.

Future developments of PEGMEMA and lithium chloride-based sensors might focus on application and optimization. A crucial aspect will be enhancing performance in extreme environmental conditions, such as high humidity or low temperatures, by integrating additives that improve reliability. At the same time, optimizing the sensor's sensitivity and durability could be achieved through studies on the effects of different additives and salt concentrations. Another interesting goal is enabling these devices to simultaneously detect deformation and temperature without interference in electrical measurements, expanding their potential applications. Integration into soft robotics and prosthetic systems represents a promising direction, as the sensor's flexibility and sensitivity allow for more precise and responsive control of exoskeletons and advanced prosthetic devices. These sensors could be used in the biomedical field to monitor physiological signals in real time, such as joint motions and muscle contractions, enhancing user comfort and the efficiency of prosthetic support. Furthermore, their use in culture platforms or bioreactors would ensure cytocompatibility and biocompatibility while allowing for real-time monitoring of tissue activity and mechanical pressures. Another key area of development involves data processing. Integrating advanced algorithms capable of analyzing and interpreting real-time data would significantly enhance the accuracy and reliability of these sensors. Additionally, advancements in photopolymerizable resins and 3D printing could facilitate the creation of customized structures tailored to specific applications. However, challenges such as cross-linking variability and sensitivity to temperature and humidity must be addressed by implementing environmental compensation strategies and stabilizing additives. Overcoming these limitations will be essential to ensuring the long-term stability and performance of these sensors. By tackling these issues, PEGMEMA-based sensors could play a crucial role in the innovation of wearable and biomedical

technologies, accelerating progress in tissue regeneration and advanced applications.

Bibliography

1. [Wearable strain sensors: state-of-the-art and future applications Ashish Yadav, Neha Yadav, Yongling Wu, a Seeram RamaKrishna b and Zheng Hongyu, Mater. Adv., 2023, 4, 1444]

2. [Flexible Wearable Sensors in Medical Monitoring Yingying Yuan 1, Bo Liu 1,2, Hui Li 3, Mo Li 3, Yingqiu Song 4, Runze W]

3. [3D Printed Stretchable Tactile Sensors, Shuang-Zhuang Guo, Kaiyan Qiu, Fanben Meng, Sung Hyun Park, Michael C. McAlpine]

4. [S. C. Mulkhopadhyway, Wearable electronics sensors for safe and healthy living, Springer, 2015]

5. [Recent Progress in Mechanically Robust and Conductive-Hydrogel-Based Sensors Ziwen Fan, Donghwan Ji, and Jaeyun Kim*]

6. [T. Q. Trung, N. E. Lee, Flexible and Stretchable Physical Sensor Integrated Platforms for Wearable Human-Activity Monitoring and Personal Healthcare, Advanced Materials, 28, 4338-4372, 2016]

7. [Fatigue Testing of Wearable Sensing Technologies: Issues and Opportunities Andrea Karen Persons, John E. Ball, Charles Freeman, David M. Macias, Chartrisa LaShan Simpson , Brian K. Smith 7 and Reuben F. Burch V.]

8. [Highly stretchable, robust, sensitive and wearable strain sensors based on mesh-structured conductive hydrogels, Ruxue Yang, Zhantong Tu, Xiyue Chen, Xin Wu]

9. [Stretchable, Skin-Mountable, and Wearable Strain Sensorsand Their Potential Applications: A Review Morteza Amjadi, Ki-Uk Kyung, Inkyu Park,* and Metin Sitti]

10. [Recent Progress in Pressure Sensors for Wearable Electronics: From Design to Applications by Yeongjun KimORCID and Je Hoon Oh, Appl. Sci. 2020, 10(18), 6403]

11. [Multimaterial Three-Dimensional Printing of Ultraviolet-Curable Ionic Conductive Elastomers with Diverse Polymers for Multifunctional Flexible Electronics Xiangnan He,Jianxiang Cheng,# Zhenqing Li, Haitao Ye, Xinfeng Wei, Honggeng Li, Rong Wang, Yuan-Fang Zhang, Hui Ying Yang, Chuanfei Guo, and Qi Ge]

12. [Liu, X.; Wei, Y.; Qiu, Y. Advanced Flexible Skin-Like Pressure and Strain Sensors for Human Health Monitoring. Micromachines 2021, 12, 695]

13. [Review Wearable Sensors for Healthcare: Fabrication to Application Subhas Chandra Mukhopadhyay, Nagender Kumar Suryadevara 2 and Anindya Nag]

14. [Ruth, S.R.A.; Beker, L.; Tran, H.; Feig, V.R.; Matsuhisa, N.; Bao, Z. Rational Design of Capacitive Pressure Sensors Based on Pyramidal Microstructures for Specialized Monitoring of Biosignals. Adv. Funct. Mater. 2019, 30, 1903100]

15. [Tee, B.C.K.; Chortos, A.; Dunn, R.R.; Schwartz, G.; Eason, E.; Bao, Z. Tunable Flexible Pressure Sensors using Microstructured Elastomer Geometries for Intuitive Electronics. Adv. Funct. Mater. 2014, 24, 5427–5434]

16. [De la Vega, A., Sumfleth, J., Wittich, H. et al. Time and temperature dependent piezoresistance of carbon nanofiller/polymer composites under dynamic load. J Mater Sci 47, 2648–2657 (2012), https://doi.org/10.1007/s10853-011-6090-7]

17. [Chen M, Luo W, Xu Z, Zhang X, Xie B, Wang G, Han M. An ultrahigh resolution pressure sensor based on percolative metal nanoparticle arrays. Nat Commun. 2019 Sep 6;10(1):4024. doi: 10.1038/s41467-019-12030-x. PMID: 31492843; PMCID: PMC6731318.]

18. [Y. Wan, Y. Wang, C.F. Guo, Recent progresses on flexible tactile sensors Mater. Today Phys., 1 (2017), pp. 61-73, doi:10.1016/j.mtphys.2017.06.002]

19. [Choi S-G, Kang S-H, Lee J-Y, Park J-H and Kang S-K (2023), Recent advances in wearable iontronic sensors for healthcare applications. Front. Bioeng. Biotechnol. 11:1335188. doi: 10.3389/fbioe.2023.1335188]

20. Choi SG, Kang SH, Lee JY, Park JH, Kang SK. Recent advances in wearable iontronic sensors for healthcare applications. Front Bioeng Biotechnol. 2023 Dec 15;11:1335188.doi: 10.3389/fbioe.2023.1335188. PMID: 38162187; PMCID: PMC10757853.]

21. [Sun L., Chen S., Guo Y., Song J., Zhang L., Xiao L., et al. (2019). Ionogel-based, highly stretchable, transparent, durable triboelectric nanogenerators for energy harvesting and motion sensing over a wide temperature range. Nano Energy 63, 103847. 10.1016/j.nanoen.2019.06.043]

22. [Liu H., Xu D., Hu B., Jiang J., Li M., Zhao D., et al. (2021). Eco-friendly biogenic hydrogel for wearable skin-like iontronics. J. Mater. Chem. A 9 (8), 4692–4699. 10.1039/d0ta12345e]

23. [Sun J.-Y., Zhao X., Illeperuma W. R., Chaudhuri O., Oh K. H., Mooney D. J., et al. (2012). Highly stretchable and tough hydrogels. Nature 489 (7414), 133–136. 10.1038/nature11409]

24. Min Gao, Rongrong Zhao, Beibei Kang, Zengdian Zhao, Shasha Song, High-performance ionic conductive double-network hydrogel enabling a long-term flexible strain sensor, Colloids and Surfaces A: Physicochemical and Engineering Aspects, Volume 663,2023,131051, ISSN 0927-7757]

25. [Jian Tang, Yuting Wu, Shidong Ma, Tao Yan, Zhijuan Pan, Sensing mechanism of a flexible strain sensor developed directly using electro spun composite nanofiber yarn with ternary carbon nanomaterials, iScience, Volume 25, Issue 10,2022, 105162, ISSN 2589-0042, https://doi.org/10.1016/j.isci.2022.105162]

26. [Persons, A.K.; Ball, J.E.; Freeman, C.; Macias, D.M.; Simpson, C.L. Smith, B.K.; Burch V., R.F. Fatigue Testing of Wearable Sensing Technologies: Issues and Opportunities. Materials 2021, 14,4070. https://doi.org/10.3390/ma14154070]

27. [Han, F.; Li, M.; Ye, H.; Zhang, G. Materials, Electrical Performance, Mechanisms, Applications, and Manufacturing Approaches for Flexible Strain Sensors. Nanomaterials 2021, 11, 1220. https://doi.org/10.3390/nano11051220]

28. [Liu X, Wei Y, Qiu Y. Advanced Flexible Skin-Like Pressure and Strain Sensors for Human Health Monitoring. Micromachines (Basel). 2021 Jun 14;12(6):695. doi: 10.3390/mi12060695. PMID: 34198673; PMCID: PMC8232132]

29. [Hammock ML, Chortos A, Tee BC, Tok JB, Bao Z. 25th anniversary article: The evolution of electronic skin (e-skin): a brief history, design considerations, and recent progress. Adv Mater. 2013 Nov 13;25(42):5997-6038. doi: 10.1002/adma.201302240. Epub 2013 Oct 22. PMID: 24151185]

30. [Wang X, Dong L, Zhang H, Yu R, Pan C, Wang ZL. Recent Progress in Electronic Skin. Adv Sci (Weinh). 2015 Jul 14;2(10):1500169. doi: 10.1002/advs.201500169. PMID: 27980911; PMCID: PMC5115318]

31. Antonia Georgopoulou and Frank Clemens, Piezoresistive Elastomer-Based Composite Strain Sensors and Their Application, ACS Applied Electronic Materials 2020 2 (7), 1826-1842 DOI: 10.1021/acsaelm.0c00278

32. Hao Meng, Weicheng Zhong, Kui Ma, Jianlong Su, Liqian Ma, Yaying Hao, Yufeng Jiang, Xi Liu, Xiaobing Fu, Cuiping Zhang,Flexible wearable sensors: An emerging platform for monitoring of bacterial infection in skin wounds, Engineered Regeneration, Volume 5, Issue 2, 2024, Pages 186-198, ISSN 2666-1381, https://doi.org/10.1016/j.engreg.2024.03.003]

33. [He X, Cheng J, Li Z, Ye H, Wei X, Li H, Wang R, Zhang YF, Yang HY, Guo C, Ge Q. Multimaterial Three-Dimensional Printing of Ultraviolet-Curable Ionic

Conductive Elastomers with Diverse Polymers for Multifunctional Flexible Electronics. ACS Appl Mater Interfaces. 2023 Jan 18;15(2):3455-3466. doi: 10.1021/acsami.2c18954. Epub 2022 Dec 20. PMID: 36538002]

34. [Kalkal, Ashish, S Kumar, Pramod Kumar, Rangadhar Pradhan, Magnus Willander, Gopinath Packirisamy, Saurabh Kumar and Bansi Dhar Malhotra. "Recent advances in 3D printing technologies for wearable (bio)sensors." Additive manufacturing 46 (2021): 102088.]

35. [Jenkins, A. (2000). Photoinitiators for free radical cationic and anionic photopolymerisation, 2nd edition J V Crivello and K Dietliker Edited by G Bradley John Wiley & Sons, Chichester 1998. pp ix + 586, £ 90.00 ISBN 0-471-97892-2. Polymer International, 49(12), 1729-1729.]

36. [3D Printed Flexible Strain Sensors: From Printing to Devices and Signals Haodong Liu, Hongjian Zhang, Wenqi Han, Huijuan Lin, Ruizi Li,Jixin Zhu,and Wei Huang, Adv. Mater. 2021, 33, 2004782]

37. [Decker C, Elazouk B (1995) Laser curing of photopolymers. In: Allen NS et al (eds) Current trends in polymer photochemistry. Ellis Horwood, New York, p P130]

38. [S. C. Ligon, R. Liska, et al., Polymers for 3D Printing and Customized Additive Manufacturing, Chemical Reviews, 2017, 117, 10212−10290]

39. [Leigh SJ, Bradley RJ, Purssell CP, Billson DR, Hutchins DA (2012) A Simple, Low-Cost Conductive Composite Material for 3D Printing of Electronic Sensors. PLoS ONE 7(11): e49365 doi:10.1371/journal.pone.0049365]

40. [Borrello J, Nasser P, Iatridis J, Costa KD. 3D Printing a Mechanically-Tunable Acrylate Resin on a Commercial DLP-SLA Printer. Addit Manuf. 2018 Oct;23:374-380. doi: 10.1016/j.addma.2018.08.019. Epub 2018 Aug 18. PMID: 31106119; PMCID: PMC6516765]

41. [Xiang-Yu Yin, Yue Zhang, Xiaobing Cai, Qiuquan Guo, Jun Yang, and Zhong Lin Wang, 3D printing of ionic conductors for high-sensitivity wearable sensors, Mater. Horiz., 2019,6, 767-780, DOI: 10.1039/C8MH01398E]

42. [X. Yin, Y. Zhang, X. Cai, Q. Guo, J. Yang and Z. Wang, 3D Printing of Ionic Conductors for High-Sensitivity Wearable Sensors Mater. Horiz., 2019, DOI: 10.1039/C8MH01398E]

43. [DLP 3D – printing of shape memory polymers stabilized by thermoreversible hydrogen bonding interactions Cosola, Andrea; Sangermano, Marco; Terenziani, Davide; Conti, Riccardo; Messori, Massimo; Grützmacher, Hansjörg; Pirri, Candido Fabrizio; Chiappone, Annalisa, APPLIED MATERIALS TODAY. - ISSN 2352-940723:(2021), p. 101060. [10.1016/j.apmt.2021.101060]

44. [Self-Powered Piezoionic Strain Sensor toward the Monitoring of Human Activities Yang Liu, Ying Hu, Jingjing Zhao, Guan Wu, Xiaoming Tao, and Wei Chen]

45. [Mu, Quanyi, Lei Wang, Conner K. Dunn, Xiao Kuang, Feng Duan, Zhong Zhang, H. Jerry Qi and Tiejun Wang. “Digital light processing 3D printing of conductive complex structures.” Additive manufacturing 18 (2017): 74-83.]

46. [Kayser LV, Lipomi DJ. Stretchable Conductive Polymers and Composites Based on PEDOT and PEDOT: PSS. Adv Mater. 2019 Mar;31(10):e1806133. doi: 10.1002/adma.201806133. Epub 2019 Jan 2. PMID: 30600559; PMCID: PMC6401235.]

47. [Chao Li a, Zecheng Yang, Jiadeng Zhu, Chunxia Gao, Mingxu Wang, Qiang Gao, Anti-freezing and moisturizing PAA/PEDOT: PSS iono gels with multiple stimulus responses for flexible wearable electronics, March 2024 European Polymer Journal 210(6):112934210(6):112934 DOI:10.1016/j.eurpolymj.2024.112934]

48. [He X, Cheng J, Li Z, Ye H, Wei X, Li H, Wang R, Zhang YF, Yang HY, Guo C, Ge Q. Multimaterial Three-Dimensional Printing of Ultraviolet-Curable Ionic Conductive

Elastomers with Diverse Polymers for Multifunctional Flexible Electronics. ACS Appl Mater Interfaces. 2023 Jan 18;15(2):3455-3466. doi: 10.1021/acsami.2c18954. Epub 2022 Dec 20. PMID: 36538002.]

49. [Zhang C, Zheng H, Sun J, Zhou Y, Xu W, Dai Y, Mo J, Wang Z. 3D Printed, Solid-State Conductive Ionoelastomer as a Generic Building Block for Tactile Applications. Adv Mater. 2022 Jan;34(2):e2105996. doi: 10.1002/adma.202105996. Epub 2021 Nov 19. PMID: 34734449.], [Samuel Smocot, Zixin Zhang, Lingzhi Zhang, Shu Guo, and Changhong Cao, Printed flexible mechanical sensors, Nanoscale, 2022, 14, 17134, DOI: 10.1039/d2nr04015h]

50. [Digital Light 3D Printing of PEDOT-Based Photopolymerizable Inks for Biosensing, Naroa Lopez-Larrea, Miryam Criado-Gonzalez, Antonio Dominguez-Alfaro, Nuria Alegret, Isabel del Agua, Bastien Marchiori, and David Mecerreyes, ACS Appl.Polym.Mater.2022,4,6749−6759]

51. [Borrello J, Nasser P, Iatridis J, Costa KD. 3D Printing a Mechanically-Tunable Acrylate Resin on a Commercial DLP-SLA Printer. Addit Manuf. 2018 Oct;23:374-380. doi: 10.1016/j.addma.2018.08.019. Epub 2018 Aug 18. PMID: 31106119; PMCID: PMC6516765]

52. [Ge Q, Chen Z, Cheng J, Zhang B, Zhang YF, Li H, He X, Yuan C, Liu J, Magdassi S, Qu S. 3D printing of highly stretchable hydrogel with diverse UV curable polymers. Sci Adv. 2021 Jan 6;7(2):eaba4261. doi: 10.1126/sciadv.aba4261. PMID: 33523958; PMCID: PMC7787492.]

53. [M. Gastaldi, F. Cardano et al, Functional Dyes in Polymeric 3D Printing: Applications and Perspectives, ACS Materials Letters 2021, 3 (1), 1-17, DOI: 10.1021/acsmaterialslett.0c00455]

54. [FROM PHOSPHINE TO PHOSPHANE OXIDES FUNDAMENTALS AND APPLICATIONS, A thesis submitted to attain the degree of DOCTOR OF SCIENCE of

ETH Zurich (Dr. sc. ETH Zurich) Presented by Debora Thöny MSc. Chemistry, ETH Zurich]

55. [https://www.sigmaaldrich.com/IT/it/product/aldrich/447935]

56. [Self Powered Integrated Tactile Sensing System Based on Ultrastretchable, SelfHealing and 3D Printable Ionic Conductive Hydrogel Mogli, Giorgio; Reina, Marco; Chiappone, Annalisa; Lamberti, Andrea; Pirri, Candido Fabrizio; Roppolo, Ignazio; Stassi, Stefano, ADVANCED FUNCTIONAL MATERIALS. ISSN 1616-301X. 34:7(2024),[10.1002/adfm.202307133]

57. [https://www.sigmaaldrich.com/IT/it/substance/acrylicacid720679107]

58. [Shuqiang Peng, Qiuquan Guo, Naveen Thirunavukkarasu, Yanling Zheng, Zian Wang, Longhui Zheng, Lixin Wu, Zixiang Weng, Tailoring of photocurable ionogel toward high resilience and low hysteresis 3D printed versatile porous flexible sensor, Chemical Engineering Journal, Volume 439,2022,135593, ISSN13858947,https://doi.org/10.1016/j.cej.2022.135593.

59. [H. T. Banks, S. Hu, and Z. R. Kenz, “A brief review of elasticity and viscoelasticity for solids,” Advances in Applied Mathematics and Mechanics, vol. 3, no. 1, pp. 1–51, 2011]

60. [https://www.asiga.com/max-x/]